THE AMERICAN MINERALOGIST
JOURNAL OF THE MINERALOGICAL SOCIETY OF AMERICA

Vol. 22 JANUARY, 1937 No. 1

ACCELERATED WEATHERING OF FELDSPARS

F. H. NORTON*

INTRODUCTION

This investigation was undertaken with the purpose of developing a method for the alteration of feldspars, which, except for the acceleration by higher temperatures, would more nearly simulate natural conditions than had previous methods. In order to carry this out, it was decided to supply fresh liquid to the sample, and to carry away the soluble reaction products in one continuous process. It was proposed at first to attempt the decomposition of certain types of feldspars with carbonic acid; and, in addition, to identify the reaction products and determine the temperature limits in order to throw more light on the origin of clays.

PREVIOUS WORK

Considerable work has been carried on in the past by geologists on the synthesis of clays and the decomposition of feldspars. In general two methods have been followed. First, the co-precipitated gels of alumina and silica are placed in a reaction chamber and heated for some time, usually with an acid. In this way finely crystallized kaolinite has been formed and detected by *x*-ray methods. The work of Noll,[1] van Nieuwenburg, Pieters,[2] Schwarz,[3] Ewell and Insley[4] have been along this line.

The second method consists in a hydrothermal treatment of feldspar in a reaction chamber with a rather high concentration of acid. Collins,[7] and later Badger and Ally,[8] have reported the production of kaolinite in this way by the use of hydrofluoric acid. Schwarz and Trageser[5,6] have reported the formation of both kaolinite and pyrophyllite by the hydrothermal treatment of feldspar with hydrochloric acid. Collins[7] attempted the decomposition of feldspar with carbonic acid at a low temperature but obtained no positive results.

In none of these methods has mention been made of a continual supply of fresh solute or the removal of the soluble reaction products as occurs in nature.

---

* Associate Professor of Ceramics, Massachusetts Institute of Technology.

PLAN OF THE INVESTIGATION

In this investigation the minerals orthoclase, anorthite, and albite were used as the original materials. These minerals after fine grinding were subjected to the action of water and carbon dioxide, the reaction being accelerated by a moderately high temperature. Arrangements were made for applying to the sample a supply of fresh carbonic acid solution and for removing the soluble reaction products in one continuous process. The altered feldspars were then studied by means of the petrographic microscope and the *x*-ray powder method to determine the resultant minerals present.

ORIGINAL MATERIALS

A potash feldspar from West Paris, Maine, containing a large proportion of orthoclase was selected for the first test. This material had the following analysis:

SiO_2	65.5
Al_2O_3	19.6
Fe_2O_3	0.8
CaO	0.4
MgO	Trace
K_2O	11.2
Na_2O	3.3

A soda feldspar, consisting principally of albite, was also used. The analysis showed:

SiO	58.53
Al_2O_3	19.59
Fe_2O_3	0.06
CaO	0.71
MgO	—
K_2O	1.29
Na_2O	9.52

The lime feldspar consisted of perfect crystals of anorthite from Miakejima, Japan. Because of the excellence and purity of the crystals no chemical analysis was deemed necessary.

The feldspar crystals were crushed and then ground with water in a porcelain pebble mill for three weeks, which reduced the fragments to a maximum size not greater than one micron. This very fine grinding was carried out in order to expose a maximum surface, and thus accelerate the rate of reaction.

APPARATUS

The reaction chamber developed for this work is shown in Fig. 1. The chamber itself is made from a piece of heavy seamless steel tubing with heads held in place by a ring of six cap crews. The chamber was made tight by means of a copper gasket about 1/16 in. thick which covered the entire ends of the reaction chamber. Into these gaskets were soldered the various copper connecting tubes. The sample, weighing about ten grams, was placed in a very thin, porous cup made of alumina, which is supported on a wire framework to elevate it just above the water level. A copper tube leads from the bottom of the chamber to a pressure gauge which indicates at all times the pressure in the chamber. The temperature in the chamber is measured by a copper-constantine thermo-couple inserted in a well near the center of the reaction chamber. The cold junction of the couple is kept in ice.

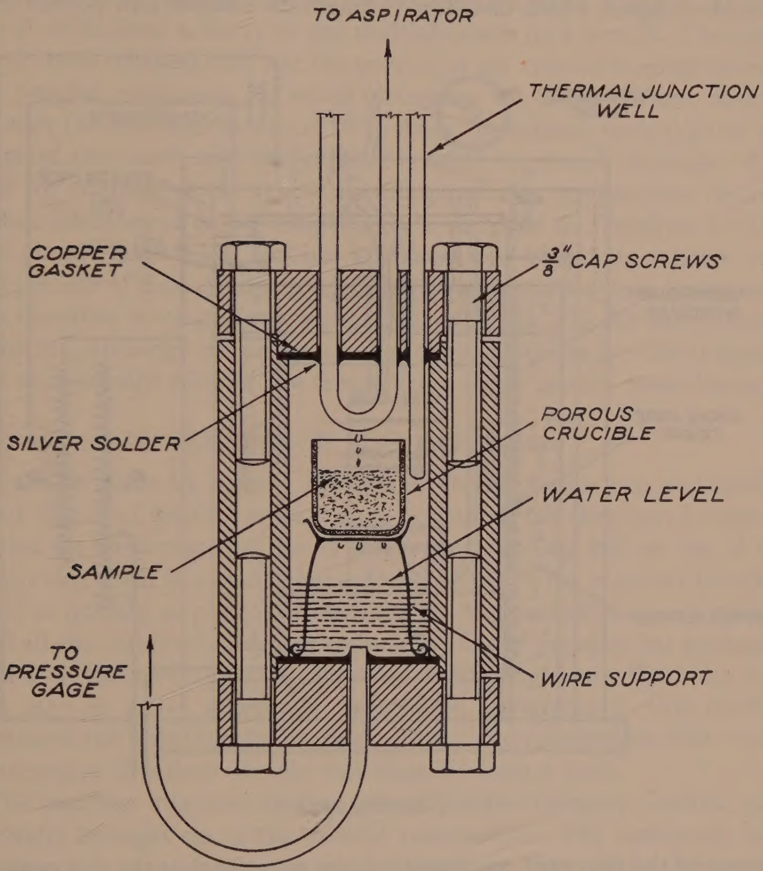

Fig. 1. Reaction chamber.

The important feature of this reaction chamber is the "U" shaped condenser tube which is silver-soldered into the top gasket. Air is drawn through this tube to condense the vapors on the outer surface from where it drips down onto the sample. The rate of condensation can be varied by the amount of air drawn through the tube. It is generally adjusted so that the rate of forming condensate is about equal to the amount of liquid which can flow through the sample and porous cup.

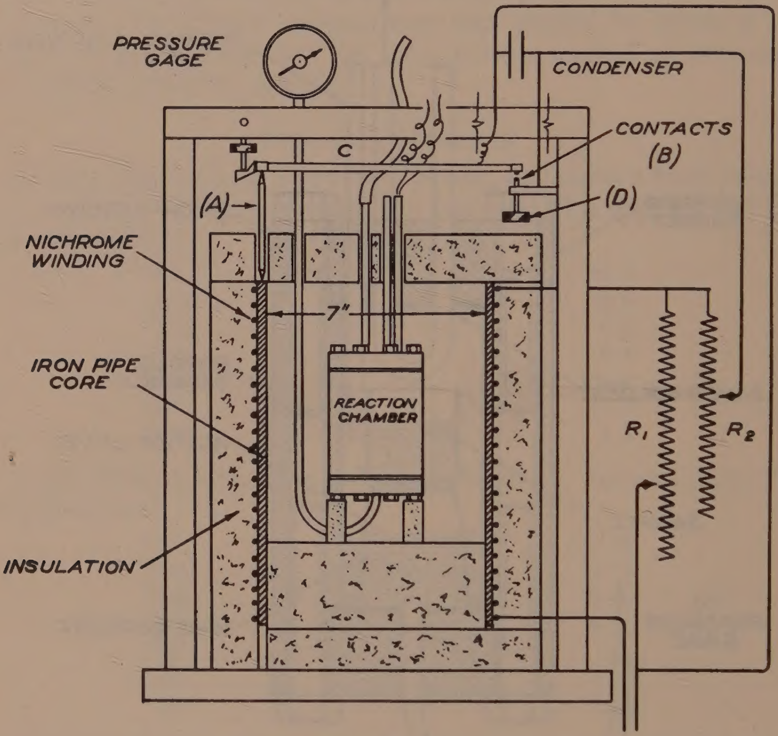

Fig. 2. Heating furnace.

In some of the first runs condensation was so rapid that the cup continuously overflowed.

One of the chief advantages of this reaction chamber is the ease with which it can be kept tight. After the first trial runs, there was little trouble with leakage, for in nearly every case the pressure when cold, at the end of a long run, was exactly the same as when the run was started. This reaction chamber before being used was tested under a hydrostatic head of 5000 pounds per square inch.

The furnace for heating the reaction chamber is shown in Fig. 2 and consists of a simple cylindrical chamber with a nichrome winding. The furnace is well insulated and requires only a few amperes to maintain the required temperature. The novel feature of this furnace is the temperature control which is shown diagrammatically in Fig. 2. An expansion of the iron furnace core acting through the strut *A* opens the contact *B* with about a thirty to one multiplication by a lever *C*. The opening of these contacts cuts out the portion of the current flowing through the parallel resistance R_2 which decreases the total current flowing through the windings by about 10%. After the furnace cools slightly the contacts are closed and the current is again increased. Rheostat R_1 is used for controlling the inflow for the particular temperature desired. A close adjustment of the temperature is obtained by the screw *D*. This very simple mechanism requires no relays and is entirely reliable over long periods of time. Under good conditions the temperature in the reaction chamber is maintained within plus or minus 1°C. for the duration of the run, although in these particular tests variations in room temperature occasionally allowed the temperature to go beyond these limits.

METHOD OF MAKING THE RUN

A run is made by placing the sample in the porous cup and adding about 75 c.c. of distilled water to the bottom of the chamber. Lumps of dry ice are then placed in the chamber, surrounding and on top of the porous cup, until it is nearly filled; then the top of the chamber is bolted down as quickly as possible. The bolts are not tightened up completely until all the carbon dioxide has vaporized and the pressure has gradually settled to the correct value. Then by tightening down the bolts it is very easy to arrive at exactly the desired gas pressure. This method eliminates the usual system of pipes, valves, and connections that would be necessary if carbon dioxide was supplied from a tank.

The reaction chamber is then placed in the furnace, covered, and gradually brought up to the desired temperature. The condenser tube is connected to an aspirator which draws air through it constantly. After the temperature is once established, the only attention required during the run is a daily check of the pressure and temperature.

RESULTS

Orthoclase

A number of runs were made with orthoclase under various conditions of temperature and carbon dioxide pressure, as shown in the following table:

TABLE 1

Run No.	Temp. C.	CO_2 Pressure Cold lbs./sq. in.	Total Pressure Hot lbs./sq. in.	Total Time at Temp.	Conversion
2	225°	15	390	11 days	Very slight alteration
4	320	200	2250	10	Slight alteration
6	280	265	1800	10	Slight alteration
6*a*	280	265	1800	21	Considerable change
6*b*	280	265	1800	33	Nearly complete change
7	320	525	2950	15	Nearly complete change
8	350	500	4000	11	Almost no alteration
9	250	500	2000	12	Slight leak

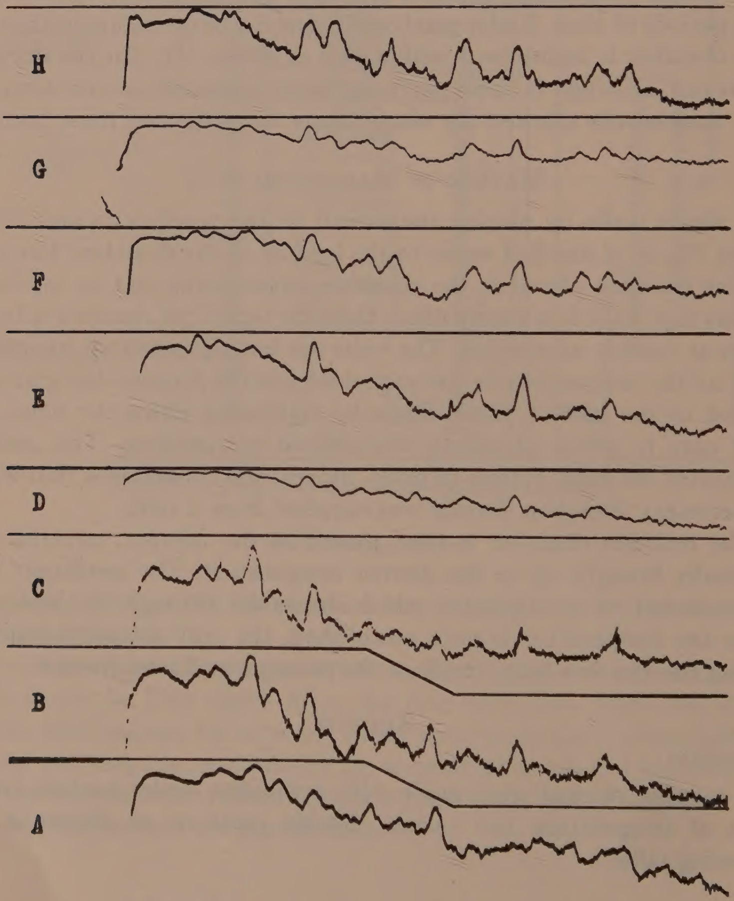

FIG. 3. Micro-photometer curves of *x*-ray patterns.

In order to determine the identity of the reaction product, x-ray patterns were made using the Cu Kα radiations from a Muller tube with a metal filter. The sample was mounted on a thread with collodion and placed in a standard Debey type camera with 57.3 mm. diameter. A .08 mm. aluminum screen was used to prevent haze in the background. As the pattern showed continuous lines, density curves were run on the Moll micro-photometer.

Curve *A*, in Fig. 3, is representative of the unaltered orthoclase feldspar. Curve *B* represents the treated sample from run No. 4, indicating a slight alteration from the original sample. Curve *C* is the product from run No. 6*a* and shows a slightly greater change from the original material. Curve *D*, from run No. 6*b*, indicates a still closer approach to the end product, although the high density of this particular negative somewhat obscures the details of the curve. Curve *E*, from run No. 7, is almost completely altered to sericite, as can readily be seen by comparing with the curves *F* and *G*, which represent muscovite and sericite. These latter curves are practically identical, although the variation in density of the negative somewhat decreases the amplitude of the peaks in curve *G*. Curve *H* represents an English china clay or kaolinite, shown in order to indicate the considerable difference from the decomposition product obtained in these runs. In fact, patterns were made from most of the hydrated aluminum silicates on the same apparatus in order to be sure that sericite alone satisfied the conditions.

An interesting fact brought out in Table 1 is that apparently no decomposition took place at 350°C., while comparatively rapid conversion occurred at 320°C. An upper temperature limit may lie between these values, above which the decomposition cannot proceed, but more work must be carried out before a definite statement can be made. As yet no definite conclusion can be drawn in regard to the influence of CO_2 pressure on the reaction.

Another check on the identity of the mineral formed can be obtained from the amount of combined water stable in the sample above 110°C. The following table shows this:

TABLE 2

Material		Ignition Loss
Orthoclase as finely ground		2.1%
Run #6	(10 hours)	4.0
Run #6*a*	(21 hours)	5.5
Run #6*b*	(33 hours)	5.9
Muscovite		6.2

It is apparent that the ignition loss increases regularly with the conversion, from 2.1% for the original feldspar to 6.2 for the sericite. These figures indicate fairly well the extent of the change.

We can also obtain some indication of the type of mineral formed in the decomposition by studying the thermal curves shown in Fig. 4. The first curve represents kaolinite with a heat absorption at 580°C. and an evolution of heat at about 970°C. The second curve is for muscovite which probably has the same crystal structure as sericite, and it will be seen that there is only a slight heat absorption around 600°C., but no heat evolution to correspond with the kaolinite. The curves for run No. 6*a* and run No. 7 indicate a considerable similarity to the muscovite, and here again there is no trace found of the heat evolution at 970°C.

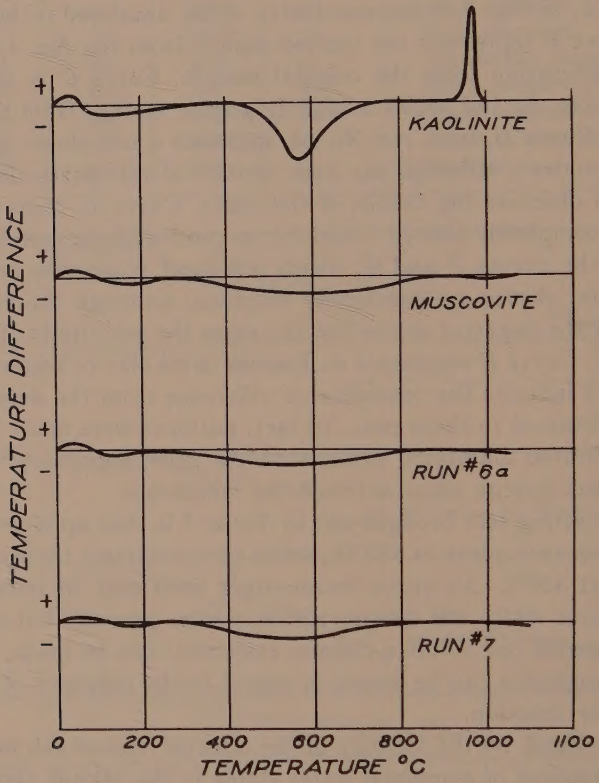

Fig. 4. Thermal curves.

Therefore we may conclude from the confirming evidence of the *x*-ray diagrams, the heating curves, and the ignition loss that orthoclase is converted quite readily to the mineral sericite at temperatures up to 320°C. We may write the following equation to express the reaction occurring in this decomposition process:

$$3[K_2O \cdot Al_2O_3 \cdot 6SiO_2] + 2CO_2 + 2H_2O \rightarrow$$
$$2[(OH)_2 \cdot KAl_2(Si_3Al)\ O_{10}] + 2K_2CO_3 + 12\ SiO_2.$$

The potassium carbonate and silica resulting from this change are taken away from the sample by the percolating water, leaving a concentration of potassium carbonate in the water at the bottom of the chamber. This silica was in the form of a hard, shiny crust firmly attached to the metal at the surface of the water. An *x*-ray film of this crust gave a definite pattern for quartz. Although no chemical analysis was made of the water left in the reaction chamber, it gave a fairly strong alkaline reaction, undoubtedly due to the dissolved potassium carbonate. In this particular feldspar, there was, of course, a certain proportion of soda, and this partially replaced the potash in the above equation.

Anorthite

Runs made on the anorthite are shown in the table below:

TABLE 3

Run No.	Temp. C.	CO_2 Pressure Cold	Total Pressure	Total Time at Temp.	Conversion
11	300	260	1950	18 days	No change
12	250	300	1230	23	Slight change
14	275	300	1650	24	Considerable change

An *x*-ray pattern of the original anorthite and the resultant product of run No. 14 is shown in Fig. 5.

It will be noted that there are two sets of lines; one dotted and one continuous. Therefore, a micro-photometer curve was not particularly satisfactory for use in analysis. The petrographical examination of the decomposition products showed a definite crystallization of calcite, and if we therefore take from the original *x*-ray pattern the lines of calcite, which are spotted due to the large size of the crystals, we find the resultant pattern agrees with that of the mineral pyrophyllite, except for one faint line which corresponds to a line from the quartz pattern. It is believed that a little quartz may have come from a slight disintegration of the bond in the porous crucible. The lines as measured on the film are shown in Table 4.

The reaction occurring in this decomposition may be expressed as follows:

$$CaO \cdot Al_2O_3 \cdot 2SiO_2 + H_2O + CO_2 \rightarrow (OH)_2Al(Si_2O)_5 + CaCO_3.$$

In this case there was no deposit of quartz around the lining of the reaction chamber as was true of the orthoclase, and there was very little evidence of the resulting calcite being carried away with the percolating water. As calcite is undoubtedly slightly soluble in water containing carbon dioxide, it seems strange that the crystals of calcite grow to such a large size in the porous cup. This may be due to the fact that the carbon dioxide was in such high concentration that it prevented any solution of the calcium carbonate.

X-ray diagram of untreated anorthite.

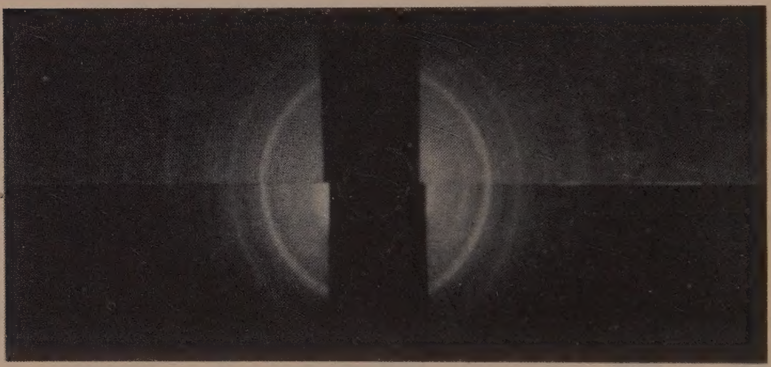

X-ray diagram of treated anorthite.

FIG. 5

The few runs that have been made seem to indicate that this reaction will not take place above 300°C., but will take place fairly rapidly at 275°C.

Table 4. Anorthite (Run #14)

Original Anorthite		Treated Anorthite		Pyrophyllite		Calcite	
Dist. in cms. on film	Intensity	Dist. in cms. on film	Intensity	Dist. in cms. on film	Intensity	Dist. in cms. on film	Intensity
		2.00	2	1.95	8		
2.30	2	2.30	3				
		2.73	1	2.75	8	2.76	0.5
2.88	10	2.84	10	2.85	8		
3.14	2	3.10	1			3.06	8
3.28	2	3.27	1				
		3.44	1	3.42	6		
3.68	5	3.64	4	3.62	6	3.76	2
3.90	0.5						
4.10	0.5	4.00	1	4.05	2	4.09	3
4.34	3	4.33	3				
4.64	3	4.60	1				
		4.82	1	4.80	1	4.89	5
		5.02	2			4.93	5
5.30	2	5.27	2				
		5.42	1	5.38	2		
5.84	0.5	5.80	1			5.79	0.5
		6.13	2	6.10	2	6.24	1
6.40	2	6.34	2	6.38	0.5		
6.56	1	6.50	1			6.47	1
6.84	1	6.84	2				
7.04	2	7.02	2				
7.56	1	7.56	1				
		7.64	1				
8.06	0.5	8.00	1				
8.40	0.5	8.33	1			8.27	1

Albite

The mineral albite was tested in the reaction chamber as indicated in the table below.

Table 5

Run No.	Temp. C.	CO_2 Pressure Cold lbs./sq. in.	Total Pressure Hot lbs./sq. in.	Total Time at Temp.	Conversion
10	315	200	2100	19 days	No change
13	250	300	1230	23	Slight change
15	275	300	1650	24	Slight change

X-ray diagram of untreated albite.

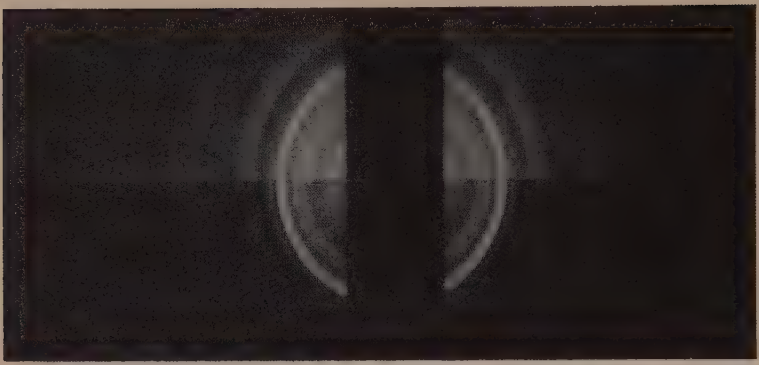

X-ray diagram of treated albite.

Fig. 6

The *x*-ray patterns for the original and altered material shown in Fig. 6 indicate a slight structural change, but not as great as for the other minerals. The reason for this slight change is not certain, as it would be supposed that this mineral would be less stable than the potash feldspar. It is possible that we have not as yet selected a temperature giving the maximum rate of conversion. Also the reaction chamber always showed a light film of oil on the water, which came from the gauge and this may have retarded the reaction. Indications of the types of reaction products are not particularly clear, but seem to suggest an alteration to the mineral paragonite, a soda mica analogous to sericite. In Table 6 are given the *x*-ray film measurements. Only sericite, of the minerals checked, showed agreement with the new lines formed, and here a number of lines are missing. No pure paragonite was available for comparison. Longer runs to decompose the albite more completely will be necessary before definite identification is possible.

Table 6. Albite (Run #15)

Original Albite		Treated Albite		New Lines		Sericite	
Dist. in cms. on film	Intensity	Dist. in cms. on film	Intensity	Dist. in cms. on film	Intensity	Dist. in cms. on film	Intensity
		2.04	6	2.04	6	2.00	10
2.24	5	2.24	6			2.20	8
2.44	5	2.44	6				

Table 6—*Continued*

		2.70	3	2.70	3	2.73	8
2.80	10	2.80	10				
3.09	4	3.07	4			3.18	0.5
3.56		3.56	6	3.56	6	3.53	10
3.74	3	3.71	3				
3.96	1	3.90	3				
4.32	3	4.30	2				
4.66	2	4.66	2			4.60	2
5.10	6	5.04	6				
		5.20	0.5	5.20	0.5		
5.58	2	5.60	4			5.62	3
5.90	1	5.92	0.5				
6.13	1	6.09	0.5				
6.27	1	6.27	6			6.32	8
6.42	2	6.44	2				
6.62	2	6.60	2				
6.87	3	6.85	2				
7.06	2	7.06	1			7.05	2
7.26	0.5	7.28	0.5				
		7.49	0.5				
		7.80	1	7.80	1	7.77	2
8.10	0.5	8.10	0.5				

DISCUSSION OF RESULTS

The upper temperature of 320°C. for the decomposition reaction found in these experiments is materially lower than that determined by Schwartz and Trageser. They state that pyrophyllite is a high temperature product, formed above 400°C., while below that temperature kaolin is produced. In the present investigation no kaolin was noted under any of the conditions of our tests. This difference may be due entirely to the comparatively low concentration of carbonic acid.

Sericite is sometimes an associate of kaolin in weathered feldspar, and by some geologists is considered an intermediate stage in the weathering process. The present tests would indicate that sericite was a final product of feldspar alteration at comparatively high temperatures; while kaolinite may be formed at lower temperatures or under more acid conditions. Much more work is necessary to get a clear understanding of the changes involved.

The reverse process, that is the change of kaolin or clay to sericite to form slates, is a common occurrence in nature. A study of this type of alteration would be of interest as it must entail the assimilation of potash from ground waters. We have at present very little information on the temperature range of this change.

CONCLUSIONS

In this investigation there has been developed a reaction chamber for carrying on the accelerated alteration of feldspars under constant temperature conditions. The reaction simulates natural conditions because fresh liquid is constantly supplied to the sample and the soluble reaction products are constantly removed.

The three feldspars tested can be decomposed with water and carbon dioxide, the orthoclase changing to sericite, and the anorthite to pyrophyllite under the particular conditions of our tests. Maximum temperature limits for this reaction have been tentatively established at 350°C. for orthoclase, and 300°C. for anorthite. Albite was partially decomposed, but the end products are not as yet identified.

FURTHER WORK

It is realized that the present work is only a preliminary survey of the alteration of feldspar, and further investigation should be continued with other types of feldspar, and over a wider range of temperature, to obtain a quantitative value for the rate of reaction. It is quite probable that the tests carried out at lower temperatures, or with lower concentrations of carbon dioxide, will form other products. It is believed that an increase in the speed of the reaction will take place by using still finer particles of feldspar, which can be obtained by separating in a centrifuge. It would also be advisable to interrupt the run periodically and regrind the reacting material to break up the rather dense crust that forms on the surface of the specimen. This regrinding would expose fresh surfaces and give the sample more permeability.

This work has been made possible by the generosity of the Geological Society of America who have allotted funds to carry out this investigation. The author takes this occasion to express his appreciation for the assistance in this matter.

BIBLIOGRAPHY

1. Noll, W., *Naturwiss.*, vol. **20**, p. 366, 1932.
2. van Nieuwenburg, C. J., and Pieters, H. A. J., *Rec. trav. chim.*, vol. **48**, pp. 27–36, 1929.
3. Schwarz, R., and Brenner, A., *Ber. deut. chem. Ges.*, vol. **56B**, pp. 1433–7, 1923.
4. Ewell, R. H., and Insley, *J. of Res., Nat. B. of Stds.*, vol **15**, p. 173, 1935.
5. Schwarz, R., and Trageser, G., *Naturwiss.*, vol. **21**, p. 252, 1933.
6. Schwarz, R., and Trageser, G., *Naturwiss.*, vol. **23**, p. 512, 1935.
7. Collins, J. H., *Mineral. Mag.*, vol. **7**, p. 832, 1928.
8. Badger, A. E., and Ally, A., *Jour. Geol.*, vol. **40**, p. 745, 1932.

A NEW METHOD OF INTERPRETATION OF PETROFABRIC DIAGRAMS[1]

HORACE WINCHELL

ABSTRACT

According to the present technique of petrofabric analysis a large personal factor enters into the interpretation of the diagrams expressing the data. Two statistical methods are described which are easily and conveniently applied to petrofabric diagrams. The results of these tests can be quickly interpreted by means of graphs accompanying the discussion, or by means of published tables. These tests tend to eliminate this personal factor.

PART I. GENERAL DISCUSSION

The purpose of this discussion is to call attention to a weakness in the present method of interpretation of the aspect of petrofabric diagrams. Briefly, this weakness is the personal factor introduced in determining the pattern of the contoured high spots. The problem is to determine the likelihood that a given diagram would be duplicated by another, the first showing significant concentrations, the second, random distribution.

Sander's technique consists of plotting the orientations of the crystal units as points on an equal area projection—a diagram which somewhat resembles a stereographic projection (8: 118–135).[2] He then contours the density of the points to bring out groupings which indicate parallel orientations. An equal area projection, like a stereographic net, represents a sphere of reference.[3] Points on it indicate critical directions such as crystallographic, tectonic, or geographic directions. A diagram containing a number of such points may be called a statistical scatter diagram. A second diagram is constructed from the scatter diagram, and shows by contours the relative density of concentration of the points.[4]

---

[1] A petrofabric diagram consists of points within a circle, contoured to bring out concentrations. It represents the orientation data of crystal units in relation to the structural setup.

[2] First numbers in parenthesis refer to numbered references in bibliography; numbers following the colon (:) refer to pages.

[3] Description and tables for the construction of the Lambert equal area projection are given in (1:71–76).

[4] This diagram is customarily contoured in the following manner (8: 118–135, 2: 22–24). Place the diagram over a sheet of coördinate paper and cover it with a sheet of plain paper. This may be done to advantage on a light table. Considering the total area of the diagram as 100 units, describe small circles of either $\frac{1}{2}$, 1, 2, or 4 units, at selected intersections of the lines of the coördinate paper. Count the number of points within each small circle and convert this to per cent per unit area; record on the topsheet at the center of the small circle. Contour lines are then drawn on this sheet, connecting points of equal density or

It is not always certain from a study of the density diagrams that the concentrations are of enough importance to be significant, as the following diagrams will illustrate.[5]

Fig. 1A is a scatter diagram and Fig. 1B the density diagram showing by contours the concentrations of the points. This diagram represents the orientations of the quartz grains in a sample of quartz schist. The specimen was chosen because of the high orientational concentration, obvious both in the scatter diagram and in the density diagram.

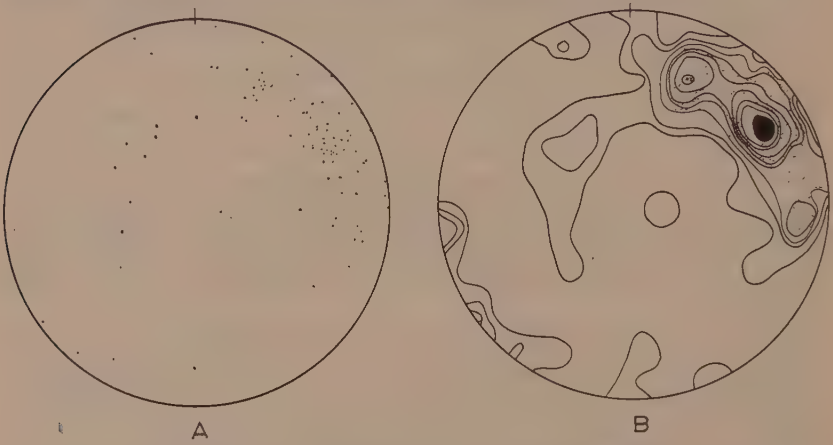

FIG. 1A. Scatter diagram. FIG. 1B. Density diagram.

FIG. 1. High concentration. Quartz schist. Petrofabric diagram of a specimen of quartz schist from Freiburg, Saxony, with 93 quartz axes. The contour intervals are 0, 1, 2, 3, 4, 5, 6 and 7, 8 and 9, 10 and 11, 12 and 13, 14% and up; the maximum is 17%. Statistical analysis gives the following results: general test $P=.000013$; zone test $P'=.000008$ (—),* .0000005 (130), .0003 (40), .048 (20). These analyses show what a remarkable concentration exists simply by the fact that the highest value of P' obtained with the zone test is .048. Slide E-10-6, University of Wisconsin petrographic collection.

* In the descriptions of this and the following figures, notations in parentheses after values of P and of P' indicate the orientation of the zone test diagram as follows: (—), as in Fig. 9*a;* (20), as in Fig. 9*b*, rotated 20 degrees clockwise; (*a.l.*), oriented about the axial line of the fold; (*a.p.*), oriented about the normal to the axial plane; (60° *a.p.*), oriented about a direction 60 degrees from the normal to the axial plane, and perpendicular to the axial line. The fold referred to is in every case the regional structure in the pre-Cambrian rocks of the Baraboo region, Sauk Co., Wis. The axial line is horizontal, striking east-west; the axial plane dips about 60 degrees north. For all diagrams of known orientation, representing specimens from the oriented Baraboo suite, the axial line is represented by the center of the diagram, and the axial plane, by the diametral line. In all the diagrams, the dotted areas represent regions of concentration of 3% or more.

---

concentration. The heaviest concentration is generally shaded to call attention to its location and distribution. The equal area projection is of course necessary because of the method of contouring used.

[5] There is necessarily a personal factor involved also in deciding the contour interval safely to be used in making density diagrams of this type. A contour interval of .2% would accentuate the maxima and bring out smaller ones, and one of 2% would perhaps conceal some important concentrations entirely. Statistical analysis of the scatter diagrams eliminates this personal factor.

Fig. 2 contains some points of doubtful concentration. It represents the orientations of some quartz axes in a specimen of deformed quartzite. In comparison with Fig. 1, this diagram seems to have no concentration at all; it remains to decide if there is any notable concentration that would be unlikely to occur in a random sample. This diagram well illustrates the difficulty of determining the correct concentration pattern without the aid of statistics.

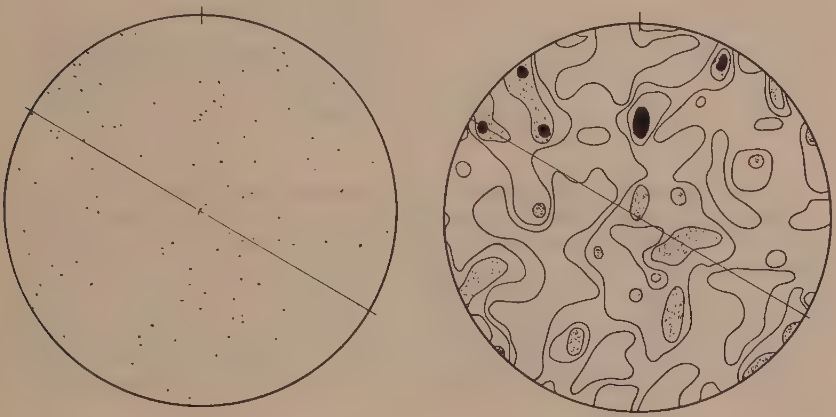

FIG. 2. Questionable concentration. Quartzite. Petrofabric diagram of a specimen of Baraboo quartzite from a fracture cleavage zone near the north end of Devil's Lake, Sauk County, Wisconsin, with 110 quartz axes. The contour intervals are 0, 1, 2, 3, 4%. Statistical analysis gives following results: general test $P=.16$; zone test $P=.18$ (*a.l.*),* .67 (*a.p.*), .21 (60° *a.p.*). As a deformed rock, this specimen might be expected to have a tectonite pattern, but no orientation of any kind is evident from the data. Results of the statistical analysis of the scatter diagram show the axes to be oriented probably at random. Specimen 20, University of Wisconsin oriented Baraboo suite, collected for the purposes of this discussion.

* See note to Fig. 1.

Figs. 3 and 4 further illustrate questionable patterns of concentration. Fig. 5 seems to exhibit at least some tendency toward a concentration in the center.

Thus it is readily seen that the present method of interpretation of petrofabric diagrams sometimes may be fully adequate; at other times it is at best only an approximation depending largely upon a personal factor; occasionally it is little better than guesswork. Statistical analysis attempts to reduce this personal factor and eliminate guesswork. This is done by means of a statistical comparison between a theoretical random distribution and the observed distribution.

The chance already mentioned that a random sample would have

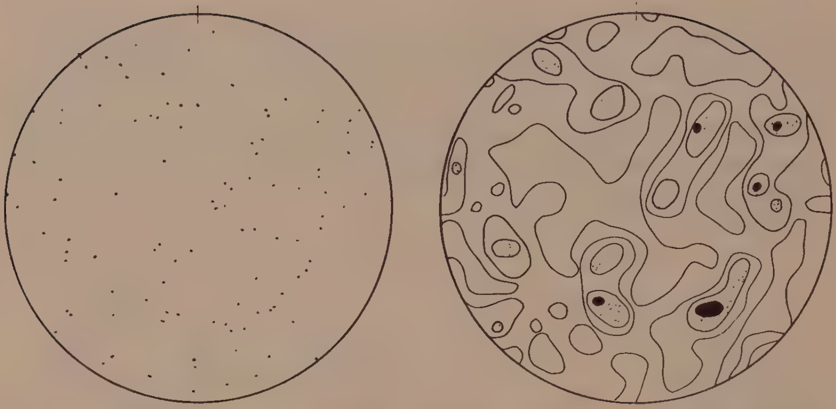

FIG. 3. Random orientation. Sandstone. Petrofabric diagram of a specimen of sandstone from the St. Peter formation (Ordovician) in a quarry in Lafayette Co., Wis., with 100 quartz axes. The contour intervals are 0, 1, 2, 3, 4%. Statistical analysis gives the following results: general test $P=.24$; zone test $P'=.83$ (−),* .91 (40). This formation and those above and below it show practically no indication of deformation of any kind. The sand grains in the St. Peter are generally rounded and frosted, and almost spherical, giving apparently ideal conditions for the production of a purely random orientation. The statistical analysis affirms this conclusion. Slide D–17–11, University of Wisconsin petrographic collection.

* See note to Fig. 1.

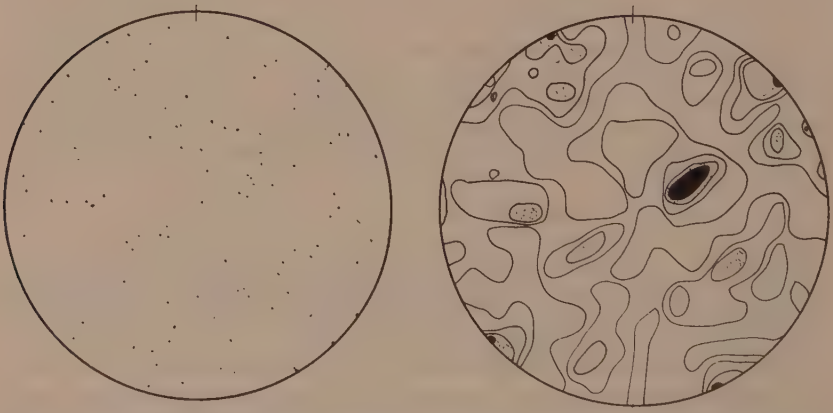

FIG. 4. Quartzite. Petrofabric diagram representing 102 quartz axes in a quartzite pebble from a conglomerate in a siliceous slate formation in the Wasatch Mountains. The contour intervals are 0, 1, 2, 3, 4, and 5%. Statistical analysis gives the following results: general test $P=.34$; zone test $P'=.86$ (−),* .66 (45). There is no indication in this diagram of any significant concentration. Specimen 15759A, slide 8151, U.S.G.S. collection at the University of Wisconsin.

* See note to Fig. 1.

concentration equal to, or greater than that of the sample in hand is, therefore, a prime concern of the structural petrologist, and it is the subject of this study. A scale for measuring this chance will be set up, the object being to remove the personal factor from the conclusions reached. This scale will be a measure of the probability that a random sample would have a divergence from a predetermined standard random, as great as, or greater than that of the sample studied. The fundamental problems to be solved are therefore first, the setting up of this theoretical random, and second, the comparison of this random with the distributions studied. The relationship between these two distributions will be expressed in terms of the probability defined above.

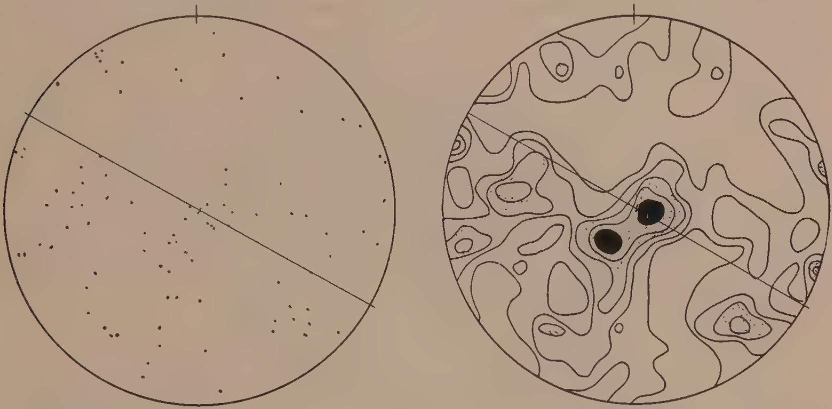

FIG. 5. Rhyolite porphyry. Petrofabric diagram of a specimen of rhyolite porphyry from the formation underlying the Baraboo quartzite, Lower Narrows, Baraboo district, Sauk Co., Wis., with 93 quartz axes. The contour intervals are 0, 1, 2, 3, 4, 5%. Statistical analysis gives the following results: general test $P=.003$; zone test $P=.055$ (*a.l.*).* 48 (*a.p.*), .37 (60° *a.l.*). This is a fairly ideal case where the general test leads to the conclusion that there is some sort of concentration, and the zone test shows the direction of the concentration. Note that only one position of the zone test axis gives a distinctly lower and more significant value of P than the other two perpendicular to it. Specimen 13, University of Wisconsin oriented Baraboo suite.

* See note to Fig. 1.

Leaving the details of the procedure to part II, some results of the various applications of the tests may be cited:

Figure 1 is shown to have a distribution of points in the scatter diagram that would happen without a controlling force only about 13 times in 1,000,000 trials—good evidence that concentration exists. This diagram, furthermore, has a zonal concentration in one direction (about a point on the periphery of the circle, 40° east of the arbitrary north marked on the diagram) such as would not be likely to occur even once in 1,000,000 trials. For comparison, the zonal concentration about another point on the periphery of the circle, 90° from the first, was tested, and it is found that the probability is less than 1 chance in 20 ($\frac{1}{20}$) of obtaining equal or greater deviation from uniformity in that direction. Ordinarily, it would be thought that the value of 1/20 might be significant, but here attention must be given to the comparison between 1/20 and 1/1,000,000.

As already remarked, Fig. 2 contains some points of doubtful concentration, a conclusion based on the usual method of interpretation. It is found, however, that about 1 time in 6 ($\frac{1}{6}$), a random sample would have just as much or more deviation from the theoretical random. This means that the chances are 1 in 6 that this rock has a purely random orientation of the quartz axes—not very convincing evidence for a significant concentration.

Figure 3 is a diagram showing the orientation of some quartz axes in a specimen of sandstone. In the region from which this sample was collected, this sandstone formation, and the formations next above and below it show no indications whatever of any deformation. The sand grains in this formation are rounded frosted quartz grains which should be ideally adapted for yielding a random orientation. The concentrations shown by the grain orientations of this specimen would be duplicated or surpassed in about 1 out of every 4 ($\frac{1}{4}$) trials.

Figure 4 represents some quartz axes in a quartzite pebble from a conglomerate in a siliceous slate formation. The statistical analysis shows that in the sample the deviation from the theoretical random would be duplicated or surpassed in about 1 out or every 3 ($\frac{1}{3}$) trials by random sampling.

Figure 5 shows the orientations of some quartz axes in a specimen of rhyolite from a zone immediately below a quartzite formation. The diagram is so oriented that the axial line of the major fold of the quartzite is at the center of the diagram, and the diametral line represents the axial plane. The concentration in this case would be duplicated or surpassed only 3 times in 1,000 (3/1000) random trials. The zonal concentration about the axial line gives a probability of only about 1 in 18 (1/18), while in two directions perpendicular to the axial line, the probability is such as to show a very uniform distribution of points with respect to these directions—the chances are about 1 in 3 to 1 in 2 ($\frac{1}{3}$ to $\frac{1}{2}$) of duplicating or surpassing this sample's deviation from uniformity in these directions.

Table 3, part II of this paper, shows these results and the results obtained on other diagrams (Figs. 10–15 inclusive). It is seen on comparing the diagrams with the results shown, that low values of the quantity P

given in the third column are usually obtained when there is any significant concentration in the diagram. The values in columns four to seven are the results of the application of a test more descriptive than the simple comparison of the observed distribution with a theoretical random distribution. Part II, containing the detailed descriptions of these tests, should be consulted for a more exact definition of the meanings of the numbers given in the table.

PART II. DETAILS OF A STATISTICAL METHOD FOR THE INTERPRETATION OF PETROFABRIC DIAGRAMS

Attention has been called to a weakness in the present technique of interpretation of petrofabric diagrams. Several instances were cited in which this weakness is apparent. The results of a statistical study were used in part for comparison with the doubtful results obtained by the standard procedure.

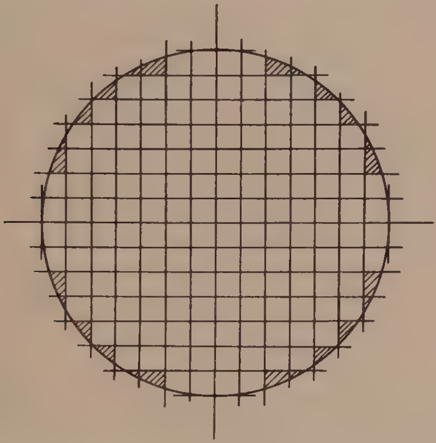

FIG. 6. Circle divided into 148 equal squares for the "general test."

It is the purpose in the second part of this discussion to describe the essential details of two statistical methods for the testing of petrofabric diagrams. In the first of these methods a theoretical random distribution of points in the petrofabric diagram is set up and compared with the distribution of points obtained by the actual study of rock thin sections. The degree of departure from random is thereby measured, the results giving a clue to the degree of concentration. The second test is a test of the departure toward a specific type of concentration located in an arbitrarily chosen direction.

For the purposes of the test to be described, the scatter diagrams (e.g. Fig. 1*A*) have been found more useful than the density diagrams (e.g. Fig. 1*B*). The diagram to be tested is divided arbitrarily into a large number of equal areas in some such manner as shown in Fig. 6. A copy of this net on transparent paper was found very useful in this procedure. This figure has 148 squares wholly or almost wholly within the circle. Superimpose it upon the scatter diagram and count the number of squares containing 0 points, the number containing 1 point, the number containing 2 points, etc., until all the squares have been counted. When a point falls on the dividing line between two squares, it must be assigned to one of them by some arbitrary rule. The rule used is commonly of the following type. Points on a north-south line are assigned to the square to the east; points on an east-west line are assigned to the square to the north. The procedure has been applied to Fig. 1 and recorded in Table 1.

TABLE 1

CALCULATION OF χ^2 FOR GENERAL TEST AS APPLIED TO FIG. 1

Formula: $\chi^2=\sum_{r=0}^{r=n}\frac{(m_r-m_r')^2}{m_r}$

Column	1	2	3	4	5	6	7
Symbol	r	m_r'	rm_r'	m_r	m_r-m_r'	$(m_r-m_r')^2$	$\frac{(m_r-m_r')^2}{m_r}$
	0	106	0	81	25	625	7.7
	1	25	25	49	24	576	11.6
	2	11	22	18	1	1	.1
	3	2	6	0*			$\chi^2=19.4$
	4	0	0	0			
	5	0	0	0			
	6	0	0	0			
	7	1	7	0			
	8	1	8	0			
	9	1	9	0			
	10	0	0	0			
	11	0	0	0			
	12	1	12	0			
		148	89	148			

$P=.005$ or less as shown by the graph.

$P=.000013$ according to tables.

* This entry could be made 3 and the one above it 15, but so small a cell frequency is not desirable in this column; much more reliable results are obtained by grouping the small numbers.

The first column shows the number of points per square; the second column shows the number of squares containing the given number of points (0, 1, 2, 3, etc.), and should of course total 148. The third column shows the number of points counted, and must be used to obtain column 4 from the graph shown in Fig. 7. Column 4 shows the theoretically most probable number of squares containing 0, 1, 2, etc., points and represents the theoretical random distribution with which the actual distribution shown in column 2 is to be compared. It is obtained from Fig. 7 as follows.[6] On the upper abscissa scale of Fig. 7, find n, the total number of points counted (sum of column 3); above this point read on the ordinate scale 148 $P_n(r)$ the vertical distance to each of the curves marked $x=0$, $x=1$, $x=2$, etc. and record the results in column 4 opposite the appropriate numbers in column 1. Curves are missing where the expectation is less than 4 squares; write 0 for each entry in column 4 corresponding to the missing portions of the curves, and increase the last number not 0 enough to make the column total 148.[7] Group together and add all the numbers in column 2 corresponding to 0's and to the last number not 0 in column 4; this sum will be compared with the

---

[6] The expected frequency of squares containing 0, 1, 2, etc., points is given by the following theorem (3: 420, 9: 455).

Let p denote the probability of the event in one trial, and q the probability of its failure. Then $p+q=1$. The probability $P_n(r)$ that the event will happen exactly r times in n trials is then

$$\frac{n!\, p^r q^{n-r}}{r!\,(n-r)!} \tag{1}$$

This is at once seen to be the formula for the rth term of the binomial expansion of $(p+q)^n$. The most probable number of squares in Fig. 6 containing r points is therefore 148 $P_n(r)$, if (as in the figure) the total number of squares is 148, and the total number of points is n. Since it is obviously impractical to calculate the value of $P_n(r)$ by this formula, a function known as Poisson's exponential is used for the purpose. Poisson's exponential function is an approximate expression for the value $P_n(r)$ in terms of e (2.718———), r, and $m(=np)$, if p is small and n large so that m is of moderate size. The expression giving $P_n(r)$ is as follows:

$$P_n(r)=\frac{e^{-m}m^r}{r!} \tag{2}$$

Tables accurate to .000001 for various values of m and r have been prepared and should be used to obtain maximum accuracy; one was used in the construction of Fig. 7 (6: table LI). For the benefit of those who wish to divide the large circle into a different number of equal areas than 148, the two auxiliary scales m and $P_n(r)$ were included. The principal scales 148 m and 148 $P_n(r)$ can be used of course only when the test diagram has exactly 148 equal areas.

[7] "In applying the χ^2 test to such a series it is desirable that the number expected should in no group be less than 5, since the calculated distribution of χ^2 is not very closely realized for very small classes" (4: 81).

last number not 0 in column 4 in place of the single number that would otherwise be used. Find the difference between corresponding entries in columns 2 and 4 and record in column 5. Square each entry in column 5 and record in column 6. Divide each entry in column 6 by the corresponding number in column 4 and record in column 7. The sum of the numbers in column 7 is "chi-squared" (χ^2).[8] If a slide rule is used, columns 5 and 6 may be omitted.

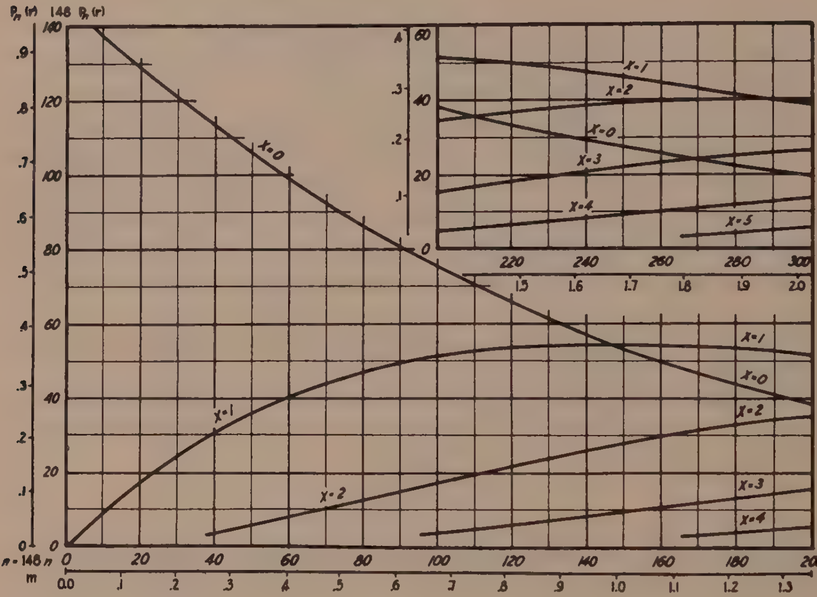

FIG. 7. Graph showing the most probable number of squares in Fig. 6 that will contain 0, 1, 2, etc., points, for any given total number of points up to 300. This graph is based on Poisson's exponential function, $P_n(r)=e^{-m}m^r/r!$. Table LI (6) was used in the construction of the graph.

---

[8] Pearson's χ^2 test for goodness of fit is based upon the equation (4, 7)

$$\chi^2=\sum_{i=1}^{i=n}\frac{(m_i-m_i')^2}{m_i}. \tag{3}$$

The value χ^2 may be converted into a probability P that a random sample would have as great or greater deviation from theory as the sample studied by means of the following formulas: (4, 6, 7)

$$P=\sqrt{\frac{2}{\pi}}\int_{\chi}^{\infty}e^{-\chi^{1/2}}d\chi+\sqrt{\frac{2}{\pi}}\,e^{-\chi^{2/2}}\left(\frac{\chi}{1}+\frac{\chi^3}{3}+\frac{\chi^{n-3}}{1\cdot 3\cdot\;\cdots\;(n-3)}\right) \tag{4}$$

for n even, and

Each entry in column 7, together with all the corresponding entries used in deriving it, constitutes one "cell" according to statistical definition. For this test, the number of cells is decreased by 2 to determine the value of n to be used in Fig. 8. Consult Fig. 8 which is a graph relating χ^2, n, and a value P, the index sought, expressing the probability that a random sample would have as great (or greater) deviation from theory as the one studied. χ^2 is located on the abscissa scale, and the vertical distance to the curve corresponding to the proper n is found on the ordinate scale P. When greater accuracy is desired, and when the graph is inadequate, tables may be used instead of the graph (4, 6, 7).

The probability index, P, may have any value between 0 and 1. It may be multiplied by 100 and expressed as per cent if desired. "If P is between .1 and .9, there is certainly no reason to suspect the hypothesis [of random distribution] tested. If it is below .02 it is strongly indicated that the hypothesis fails to account for the whole of the facts. We shall not often be led astray if we draw a conventional line at .05 and consider that higher values of χ^2 [i.e., lower values of P than .05] indicate a real discrepancy" (4: 77). In other words, if P is found to be less than .05, it is reasonably safe to conclude that there is a significant deviation from the theoretical random distribution postulated. No definite limit of this nature can logically be set, but for the purposes here discussed a limit may be chosen arbitrarily, based upon the experience of the operator and the suggestion of the statistician.

This method of determining the degree of scatter was applied to a number of petrofabric scatter diagrams; the results obtained are, as already stated, in agreement with the interpretations which would ordinarily be made concerning these diagrams, but they give a much more definite index of the degree of scatter. Figs. 1 to 5 have already been discussed. Fig. 11 gives a value of $P = .00027$, showing definite evidence of

---

$$P = e^{-\chi^2/2}\left(1 + \frac{\chi^2}{2} + \frac{\chi^4}{4} + \cdots + \frac{\chi^{n-3}}{2\cdot 4\cdot \,\cdots\, (n-3)}\right) \tag{4}$$

for n odd. n is the number of degrees of freedom in determining cell frequencies; for the zone test described later it is 9, for 9 of the cells can be filled arbitrarily and the last one is then the remainder necessary to make up the correct total number of points. n is 2 less than the number of cells in the general test described, because in addition to this first limitation, that the total number of points must fulfil a condition, the number of squares counted must also fulfil the condition of totalling 148, making two limitations instead of one. (4) Tables giving the values of P for various values of n and χ^2 have been prepared (4, 6: table XII, 7). In using such tables, it should be remembered that where some authors (e.g. 4) give n, the number of degrees of freedom, others (e.g. 6) give a value n' which is equal to $n+1$. In most cases, as in the zone test about to be described, the value n' is the number of cells.

orientation; other figures give values which are recorded in column 3 of table 3. The values given in this table suggest that every diagram studied probably has significant orientation except Figs. 2, 3, 4, 10, 12, and 13.

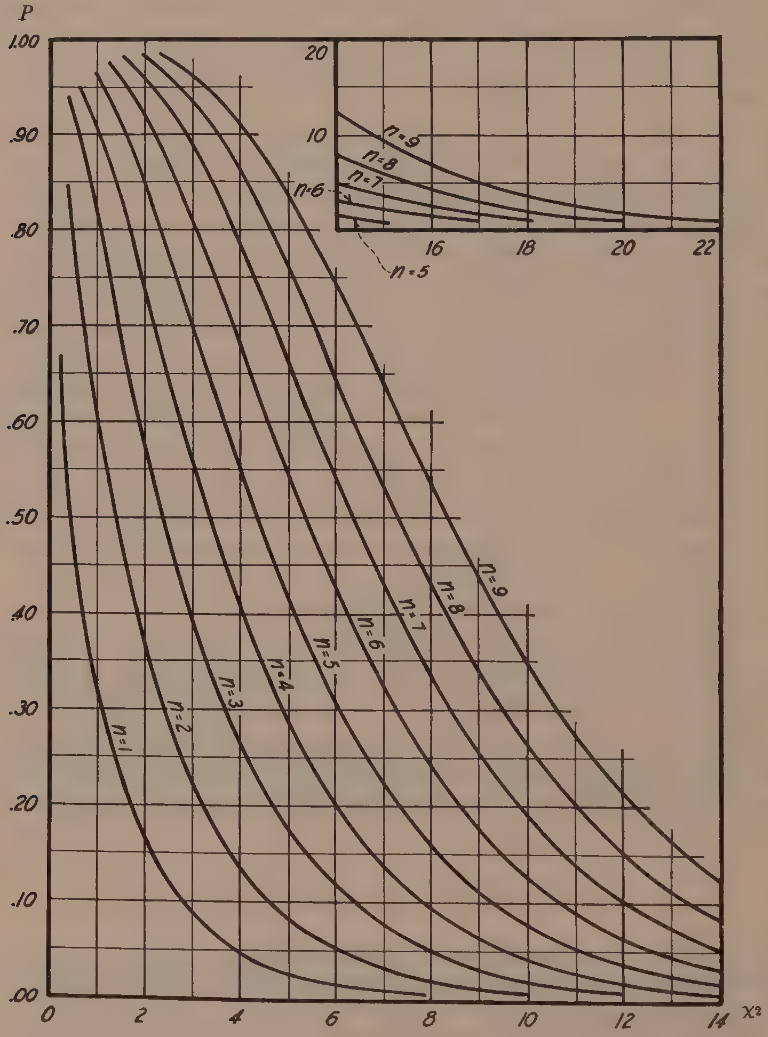

FIG. 8. Graph showing the probability that a random sample would deviate as much or more from the theoretical sample as the sample studied. This graph is based on equations (4), and was constructed from Table XII (6). Equivalent tables are given by Fisher (4), and are referred to by Rietz (7) as follows:

Elderton, W. P., *Biometrika*, 1: 155–63.

Elderton, W. P., *Tables for Biometricians and Statisticians*, pp. 26–29.

An unusually high value of P should often be considered a hint to lead to further investigation, though less definite in its meaning than a low value would be. If P is as high as .9, some significant force may often be suspected, acting to produce a distribution more nearly in agreement with the theoretical distribution than is likely to occur in random sampling. A value somewhere in the vicinity of .5 is the strongest indication of random, meaningless distribution of the points on the scatter diagram.

Since the general test just described reveals only the likelihood that the orientation is that of a random sample, and since it does not give positive descriptive results, it is in some respects inadequate. Another test was therefore devised which is believed useful in determining the nature of the orientation with respect to field relations, but necessitates certain limitations in its use. For this purpose, a circle of the size of the standard diagram was divided into ten concentric rings of equal area, as in Fig. 9*a*. These rings represent zones of equal area on the surface of the sphere of reference. This figure is superposed upon the scatter diagram in which concentration is to be tested in any zone parallel to the periphery of the diagram or around the center of the diagram,—that is, in any one or more of the delimited areas.

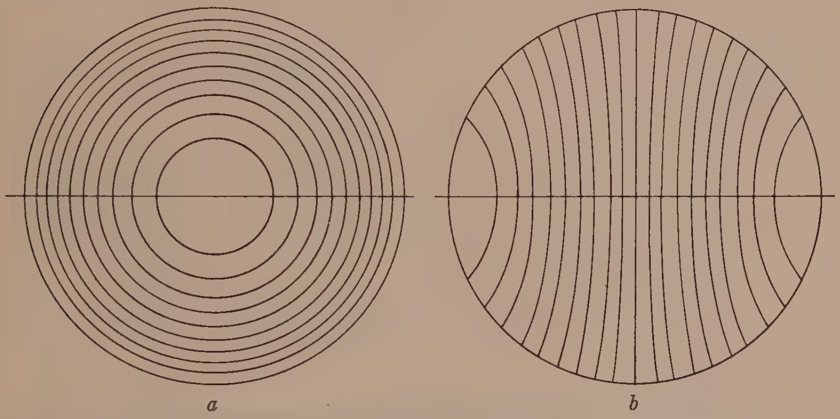

Fig. 9*a*. Circle divided into 10 rings of equal area for the "zone test."
Fig. 9*b*. Same, rotated 90 degrees about a north-south axis.

Let Fig. 5 be chosen for testing by this method. The areas are numbered from 1 to 10 starting at the center. A line is drawn diametrically across the test diagram in any arbitrary position, as shown in the figure; points on one side of this line falling on circular dividing lines are assigned arbitrarily to the higher numbered zone, and those falling on circular dividing lines on the other side of the diameter are assigned to the lower numbered zone. Table 2 is a convenient form for the tabulation of the following procedure. Column 1 shows the zone numbers—1, 2, . . . , 10. Column 2 shows the number of points counted within each zone. This column is summed and the result divided by 10 to obtain the average number of points per zone; the decimal should be retained. The third column contains the differences between the entries of column 2 and the average of column 2. Column 4 is obtained by squaring the numbers of column 3. The sum of column 4 is divided by the average of column 2 to obtain χ^2; n is 9, and a value P is obtained from Fig. 8.

TABLE 2

CALCULATION OF χ^2 FOR ZONE TEST AS APPLIED TO FIG. 5

$$\text{Formula: } \chi^2 = \sum_{r=1}^{r=n} \frac{(m_r - m_r')^2}{m_r}$$

Column	1	2	3	4	
Symbol	r	m_r'	$(m_r - m_r')$	$(m_r - m_r')^2$	
	1	19	9.7	94.0	
	2	6	3.3	10.9	$93/10 = 9.3 = m_r$
	3	6	3.3	10.9	
	4	7	2.3	5.3	$\chi^2 = 154.1/9.3$
	5	10	.7	.5	$= 16.6$
	6	10	.7	.5	$n = 9$
	7	11	1.7	2.9	$P = 0.055$
	8	6	3.3	10.9	
	9	6	3.3	10.9	
	10	12	2.7	7.3	

If P is to have a meaning comparable to that ascribed to it in the previous test—namely the probability that a random sample would have as great (or greater) deviation from the theoretical distribution postulated, as the sample studied—then the test circles must be oriented on a basis of field evidence.[9] The P determined by orienting the zone test diagram on the basis of evidence shown by the scatter diagram or by the density diagram has not the same meaning as that determined when the zones are located by the use of *a priori* evidence, such as field evidence. The meaning of the P determined with the zones oriented on the basis of evidence from the diagram is not known.

For instance, in Fig. 5, the field evidence upon which the orientation of the test diagram is based is the fact that the center of the diagram represents the direction of the axial line of the fold affecting the quartzite formation overlying the rhyolite from which the sample was taken. Thus it is tested whether there is any concentration, not in the center of the diagram, but parallel to the axial line of the fold (or in a zone around it). The resulting $P=.055$ shows that in about 1 out of every 18 trials, a random sample would have equal or greater concentration of this type.

---

[9] In spite of considerable time and energy spent upon the problem of determining the probability that a random sample would lead to as great (or greater) concentration for at least one circular region of given radius or for at least one location of a zone of fixed dimensions, as a given sample, Professor M. H. Ingraham of the Department of Mathematics of the University of Wisconsin was unable to find the solution. He consented to the use of his name as authority here.

TABLE 3

RESULTS OF APPLICATION OF THE TESTS TO SOME PETROFABRIC DIAGRAMS

1	2	3	4	5	6	7
		P—general test	P—zone test	P—zone test	P—zone test	P'—zone test
Fig. 1	93	.000013				.000008 (−)
						.000000+ 130
						.0003 40
						.048 20
2	110	.16	.18	.67	.21	
3	100	.24				.83 (−)
						.91 40
4	102	.34				.86 (−)
						.66 145
5	93	.003	.055	.48	.37	
10	105	.31	.00034	.18	.60	
11	104	.00027				.014 (−)
						.123 65
12	100	.10				.94 (−)
						.12 145
						.92 55
13	57	.35				.82 (−)
						.65 80
						.77 170
14	100	.01	.98	.42	.0035	
15	127	.001	.63	.58	.03	

In column 7, (−) after the value of P' indicates that the zones were oriented as in Fig. 9*a;* numbers after the values of P' indicate the number of degrees rotation clockwise, from the position of Fig. 9*b*.

If the concentration to be tested is not centered in the diagram, then either the test diagram or the scatter diagram must be rotated into a more favorable position. Such a rotation of the test diagram has been carried out as shown in Fig. 9*b*.

This method of testing has been applied to the diagrams already studied by means of the general test first described, and the results tabulated with those of that test. It is to be emphasized again that the best use of this test is to study concentrations in relation to field data, that is, to test the zonal concentration about predetermined directions such as a specific tectonic axis, or a specific geographic direction.

Table 3 contains the results of the application of these two tests to the diagrams shown in Figs. 1–5 and 10–15 inclusive. Column 1 shows the diagram number; column 2, the total number of points on the scatter diagram (number of quartz axes measured), and column 3, the result of the application of the general test. The remaining columns show results of the application of the zone test as follows. Column 4, the result of testing with the zones oriented about the axial line of the fold in the Baraboo quartzite formation from which or near which the specimens were taken; column 5, with the zones oriented about the direction normal to the axial plane, and column 6, with the zones oriented about a direction perpendicular to the axial line and 60° from the normal to the axial plane. Column 7 shows values designated P' to distinguish them from P with which they are not comparable, as explained above. These values were obtained by means of the same procedure, but without the use of field evidence to orient the zone test diagram.

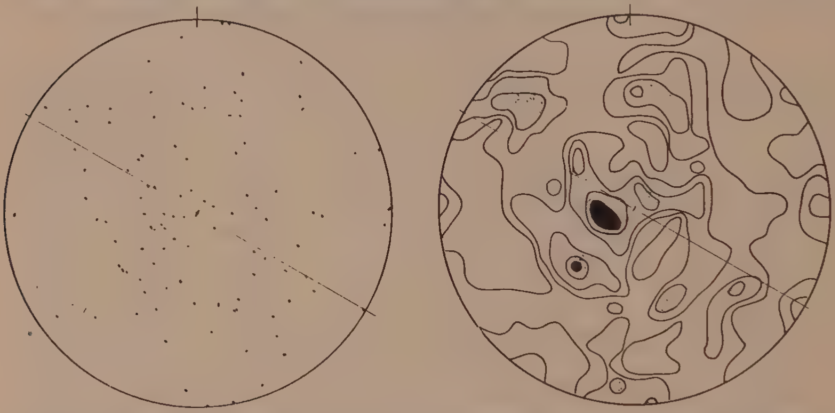

FIG. 10. Quartzite. Petrofabric diagram of a specimen of quartzite from the Baraboo formation, Devil's Lake, Sauk Co., Wis., with 105 quartz axes. This specimen was taken from a massive bed of quartzite below and adjacent to the fracture cleavage zone from which the specimen of Fig. 2 was obtained. The contour intervals are 0, 1, 2, 3, 4, 5%. Statistical analysis gives the following results: general test $P=.31$; zone test $P=.00034$ (*a.l.*),* .18 (*a.p.*), .60 (60° *a.p.*). Specimen 21, University of Wisconsin oriented Baraboo suite.

* See note to Fig. 1.

As already stated, every diagram except Figs. 2, 3, 4, 10, 12, and 13 has a value of P in column 3 (general test) which suggests orientation of some sort. The actual orientation is shown to a considerable extent in columns 4 to 7. An example will illustrate.

The general test on Fig. 14, for instance, gives a value of $P=.01$ which is significant.[10] Concentration here is shown by the zone test centered about a direction 60° from the normal to the axial plane and perpendicular to the axial line of the fold in the quartzite associated with the rhyolite porphyry from which the specimen was taken. The two other values obtained with the zone test, .98 and .42, show that there is an unusually uniform distribution of points with respect to the axial line orientation of the diagram, and approximately normal random distribution with respect to the orientation normal to the axial plane.

Figure 10 is an example of very nice Poisson distribution ($P=.31$, column 3), but a considerable concentration is shown about the axial line of the fold ($P=.0003$, col. 4), and rather even distribution perpendicular to this ($P=.18$, a.p., $P=.60$, a.p.).[11] The seemingly anomalous results of the application of the two tests to Fig. 10 do not invalidate either of them. The zone test shows with considerable assurance that there is concentration about the axial line. Although the general test fails to show evidence of this concentration, because it does not take into account the position or distribution of the squares, but only the numbers of

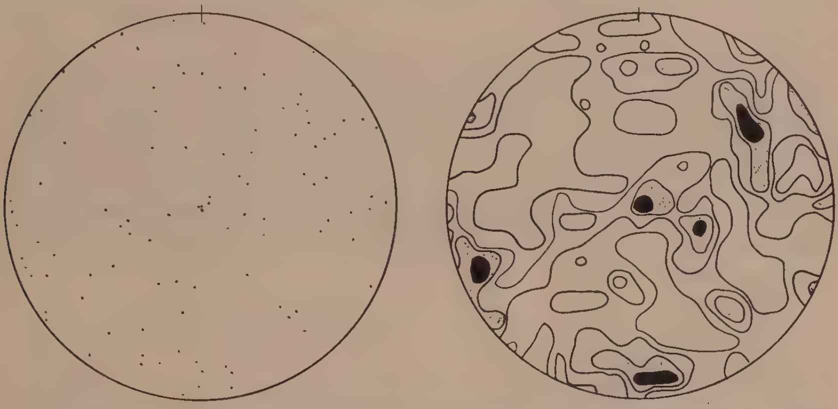

FIG. 11. Quartzite. Petrofabric diagram of a specimen of quartzite showing enlargement of the grains, taken from the vicinity of the Chapin Mine, Iron Mountain, Mich., with 104 quartz axes. The contour intervals are 0, 1, 2, 3, 4%. Statistical analysis gives the following results: general test $P=.00027$; zone test $P'=.014$ (−),* .12 (65). The general test proves considerable concentration somewhere, and the zone test shows the direction of the orientation. It is not unlikely that a different orientation of the zones, intermediate between the positions of Figs. 9*a* and 9*b*, would give even more striking values of P' than the position indicated. Specimen E-10, University of Wisconsin metamorphic collection.

* See note to Fig. 1.

---

[10] Fisher believes that values less than .02 are surely significant, and values less than 0.5 are usually significant (4: 77).

[11] See note to Fig. 1.

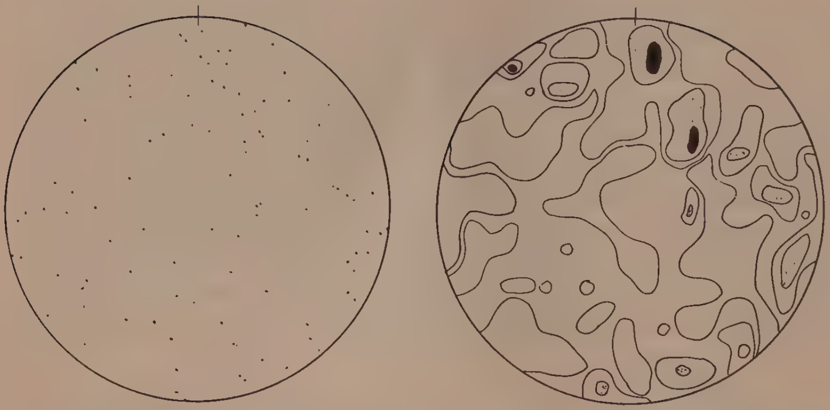

FIG. 12. Marble. Petrofabric diagram of a specimen of marble from Ashley Falls, Mass., with 100 calcite axes. The contour intervals are 0, 1, 2, 3, 4%. Statistical analysis gives the following results: general test $P=.10$; zone test $P'=.94$ (−),* .12 (145), .92 (55). The zone test shows that with respect to two positions, the distribution is very uniform, and with respect to the third at right angles to both of these two, the distribution is not as uniform. A more detailed study, involving several times as many points, might possibly bring out a concentration which would be significant. Specimen L–15, University of Wisconsin metamorphic collection.

* See note to Fig. 1.

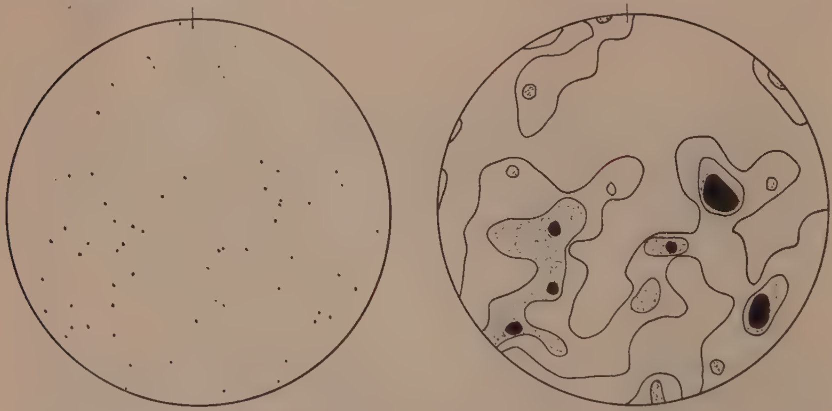

FIG. 13. Quartzose slate. Petrofabric diagram of a quartzone phase in some slates near Deadwood, S. D., with 57 quartz axes. The contour intervals are 0, 1.8, 3.5, 5.3%. Statistical analysis: general test $P=.35$; zone test $P'=.82$ (−),* .65 (80, .77 (170). The general test and the zone test in all three positions all indicate random distribution of orientation. The results of the zone test show that the distribution is very uniform in every respect. In view of the statistical data, it is doubtful whether a greater number of grains measured would discover any significant orientation. Specimen 14849, slide 7610, U.S. Geol. Survey collection.

* See note to Fig. 1.

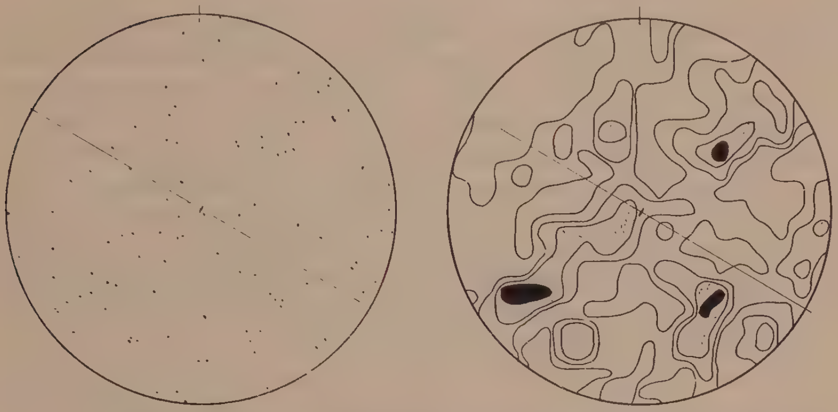

FIG. 14. Rhyolite porphyry. A petrofabric study of a specimen of rhyolite porphyry from the formation underlying the Baraboo quartzite, Lower Narrows, Sauk Co., Wis., with 100 quartz axes. The contour intervals are 0, 1, 2, 3, 4, and 5%. The statistical analysis gives the following results: general test $P=.01^{-}$; zone test, $P=.98$ (*a.l.*),* .42 (*a.p.*). .0035 (60° *a.p.*). The tests show clearly that concentration exists for the third orientation of the zone test. The density diagram helps determine which zone or zones are important regions of concentration. Specimen 14, oriented Baraboo suite.

* See note to Fig. 1.

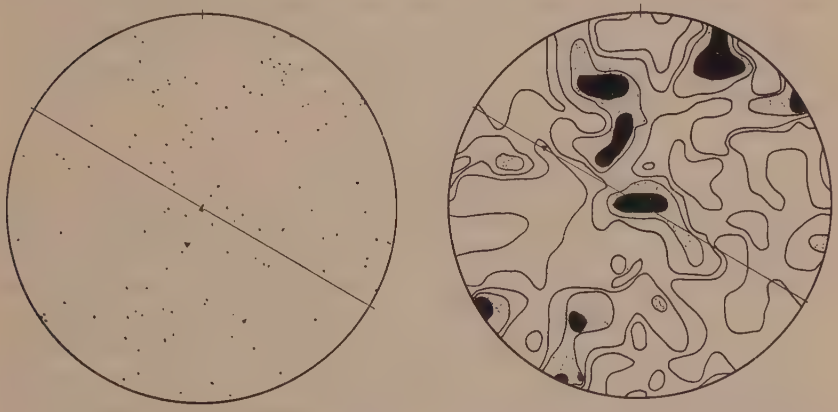

FIG. 15. Quartzite. A petrofabric study of a sample of quartzite from the Baraboo formation, Devil's Lake, Sauk Co., Wis., with 127 quartz axes. The contour intervals are 0, 0.8, 1.6, 2.3, 3.1 and 3.9%. The results of the statistical analysis are as follows: general test $P=.001$; zone test $P=.63$ (*a.l.*),* .58 (*a.p.*), .03 (60° *a.p.*). An interesting comparison can be made of the results of the statistical tests as applied to this figure, and to figures 2 and 10; these three samples represent samples of adjacent beds. The fracture cleavage zone in the middle shows no concentration; the massive bed below it shows concentration in a different direction. Specimen 19, University of Wisconsin oriented Baraboo suite.

* See note to Fig. 1.

them, containing 0, 1, 2, etc., points, this test does give definite evidence useful in describing the kind or type of concentration further. For the concentration is now describable, not only in its relation to the axial line of the fold (or to the areas of the zone test), but also in its distribution type, as shown by the general test. The general test has shown that concentration to be not remotely different from the Poisson distribution used as a basis of comparison. This is an example of one of the inadequacies of the general test; the writer has no knowledge or experience to show whether it is to be considered a frequent occurrence, but it is the only such example found in a series of 12 petrofabric studies made in connection with the development of these tests.

It is not to be overlooked that this zone test is equally applicable to diagrams having either point, or girdle concentration. Thus it can be used with *b*-tectonites as well as with *s*-tectonites.

Acknowledgment

The writer is under special obligation to Professor R. C. Emmons of the Geology Department of the University of Wisconsin for his critical reading of the paper, and for his aid and suggestions as to presentation, and to Professor M. H. Ingraham, Chairman of the Mathematics Department of the University of Wisconsin, who spent much time in the consideration of the statistical problems involved in this study. The writer expresses thanks also to his father, Professor A. N. Winchell, of the Geology Department, and to other members of the faculty of that department, for their suggestions and interest.

Summary

Petrofabric analysis as discussed in this paper is the detailed study of the orientation of selected minerals in a rock section, leading to conclusions concerning parallelism or tendencies toward parallelism of orientation of these grains. The orientations of individual grains are indicated by points on an equal area projection, and the diagram is contoured to show the density of concentration of these points. This contouring method of interpreting the data introduces a personal factor which can be largely eliminated by the use of the proper statistical tests. Such a test has been devised and its application to a number of petrofabric diagrams has been described. The test measures the probability that a random sample would have concentrations equivalent to, or greater than those of the sample studied.

The results of applying the tests to a series of diagrams prepared from oriented and non-oriented slides cut from specimens of tectonites and non-tectonites are tabulated, showing that the tests are capable not

only of determining simply the degree of departure from random, but also to a certain extent at least, of describing the concentration with respect to its direction and degree.

APPENDIX. *Descriptions of samples collected for the purpose of this paper, from the vicinity of Baraboo, Sauk Co., Wis.*[12]

To record the orientation of specimens, two arrows were made on each with colored pencils, after first knocking the sample free, trimming slightly, and then fitting back into its original position. A red arrow was in every case made horizontal, and its compass direction recorded. A blue arrow pointing upward was made perpendicular to the red one, and its dip recorded.

Each thin section was cut with the intention of orienting it so as to lie in a vertical plane striking north, with the arrow marked on it in such a position as to be in a horizontal plane and pointing north. Since the rocks of the Baraboo district form an asymmetric fold with a horizontal east-west axial line and with its axial plane dipping about 60 degrees north, the resulting thin sections are approximately normal to the axial line, and the normal to the axial plane lies 30 degrees from the arrow. The average error of orientation of the thin sections is probably not more than 10 degrees in any direction. The position of the arrow, i.e., on the east or the west side of the thin section is recorded.

Specimens 1 to 17 inclusive are from the vicinity of the Lower Narrows, Baraboo River, near the town of Baraboo, Sauk Co., Wisconsin. Specimens were taken at varying elevations, mostly in the middle one-third of the hill, on the west nose. They were located by their approximate distance in meters north or south from the center of the depression which represents the contact between the Baraboo quartzite formation and the rhyolite porphyry underlying it. Those specimens marked with an asterisk (*) are of questionable orientation. The first number refers in each case to the specimen number, the second to the distance in meters north (N) or south (S) from the contact; the third notation is a brief description of the nature of the rock; following this are the notations describing the position of the red (horizontal) and blue (in vertical plane normal to red) arrows marked on the specimen. The last notation refers to the east (E) or west (W) side of the thin section, and indicates the side on which the arrow is marked. This notation is also carried out in the description of specimens 18 to 21, except that the location is completely described.

[12] Designated *U. W. oriented Baraboo suite.*

1	21	S	massive quartzite: red N 8 W, blue 83 W: E
2	15	S	massive quartzite: red N 73 E, blue 77 M: E
3	20	S	quartzite: in fracture cleavage zone; fracture cleavage dip 60 N strike N 85 W, bedding dip *ca.* 90 strike N 75 E: red N 23 W, blue 81 W: E
*4	3	S	vein quartz, sheared quartzite: red N 3 W, blue 77 E: W
*5	11	S	quartzite: red N 75 W, blue 87 S (X on top side): W
6	8	S	quartzite: red S 38 W, blue 59 W: ?
*7	5	S	quartzite: red N 10 W, blue 87 E: E
8	3	S	quartzite: red N 13 W, blue 87 E: W
9	2	S	quartzite: red N 45 E, blue 60 W: W
10	2	S	quartzite: red N 52 W, blue 48 E: W
11	2	N	rhyolite: schistosity N 75 W dip 45 N, red N 78 W, blue 73 S: W
12	5	N	rhyolite etc: red N 65 E, blue 90: fragment chipped, W or E not certain; if W, arrow ok, if E, arrow reversed; arrowhead not certain.
13	10	N	rhyolite, etc: red N 25 W, blue 74 N: W
14	20	N	rhyolite porphyry: red N 78 E on bottom of sample; blue 39 N: W
15	30	N	rhyolite etc: red N 10 E, blue 87 E: W
16	50	N	estimated, rhyolite etc: red N 15 E, blue 45 E: E
17	85	N	estimated, rhyolite etc: red N 44 W, blue 90: E
18			Located about 2 miles W of Lower Narrows on N side of N range; sample shows various joint system directions; joint systems very well developed; major joint or bedding plane N 5 E dip 26 W; striations on this plane, direction N 30 E to N 5 E: red N 35 E, blue 62 N: line is in N–S direction, but arrowhead is not known and line may be on E or W side of thin section.
19–21			inclusive: Located at small zone of fracture cleavage near base of E Bluff, behind the cottages at the N end of Devil's Lake.
19			upper massive quartzite bed, contiguous to bed showing fracture cleavage: red N 35 W, blue vertical: W
20			fracture cleavage zone: red N 35 W, blue vertical: W
21			lower massive quartzite bed, contiguous to beds howing fracture cleavage: red N 25 E, blue vertical: W

BIBLIOGRAPHY

1. Deetz, C. H., and Adams O. S., Elements of Map Projection: *United States Coast and Geodetic Survey*, Serial no. **146**, Special publication no. 68, Washington, D.C., 1934.
2. Fairbairn, H. W., *Introduction to Petrofabric Analysis:* Department of Geology, Queen's University, Kingston, Canada, **1935.**
3. Fine, H. B., *College Algebra:* Ginn and Co., Boston, **1904.**
4. Fisher, R. A., *Statistical Methods for Research Workers:* Oliver and Boyd, London, **1934,**
5. Leith, C. K., Rock Cleavage: *U. S. Geological Survey*, Bulletin **239,** Washington, D.C., 1905.
6. Pearson, K., *Tables for Statisticians and Biometricians:* Cambridge University Press, **1914.**
7. Rietz, H. L., Editor, *Handbook of Mathematical Statistics:* Houghton Mifflin Co., New York, **1924.**
8. Sander, B., *Gefuegekunde der Gesteine:* Julius Springer, Vienna, **1930.**
9. Todhunter, I., *Algebra:* Macmillan and Co., London, **1873.**

THE MELTING OF DANBURITE:* A STUDY OF LIQUID IMMISCIBILITY IN THE SYSTEM, $CaO–B_2O_3–SiO_2$

G. W. Morey and Earl Ingerson,
Geophysical Laboratory, Washington, D.C.

In an orienting study of the quaternary system, $Na_2O–CaO–B_2O_3–SiO_2$, Morey[1] found that the mineral danburite, $CaO \cdot B_2O_3 \cdot 2SiO_2$, melts with formation of two liquid layers. Since in each of the two limiting binary systems, $CaO–SiO_2$,[2] and $CaO–B_2O_3$,[3] there is a range of composition within which two layers are formed, it was inferred that a band of immiscibility extends across the ternary system, $CaO–B_2O_3–SiO_2$. Our study has confirmed that inference, and brought out other facts which make this system one of unusual interest.

1. The Immiscible Liquids

In the binary system, $CaO–SiO_2$, Greig[2] found that the limits of immiscibility are from 27.5 to 0.6% CaO. The composition of the lighter layer was estimated from the refractive index of the glass, which was 1.460+ for the liquid which separated at 1700°. Carlson[4] found the immiscibility in the system, $CaO–B_2O_3$, to extend from 23 to 0.2 per cent CaO. In the binary system, $B_2O_3–SiO_2$, there is no indication of immiscibility. Homogeneous glasses can be obtained over the entire range of composition by mixing, repeated grinding and subsequent fusion, but mixtures high in SiO_2 are difficult to obtain as homogeneous glasses because of the volatility of boric oxide at the high temperatures required.[5] The glasses have refractive indices[6] and densities[7] lower than correspond to an additive relationship between the two components.[8]

When CaO is added to the binary system, $B_2O_3–SiO_2$, it immediately results in the formation of a second liquid phase. CaO is almost insoluble in the layer richer in boric oxide and silica, which is the layer of lower density and refractive index. The amount of CaO dissolved is not sufficient to raise the index to 1.46.

---

* Presented at the New York Meeting of the Mineralogical Society, Dec. 26, 1935. Abstract, *Am. Mineral.*, vol. **21**, p. 194, 1936.

[1] Morey, G. W., *Jour. Am. Ceram. Soc.*, vol. **15**, p. 457, 1932.

[2] Greig, J. W., *Am. Jour. Sci.*, vol. **13**, p. 1, 1927.

[3] Guertler, W., *Zeit. anorg. Chem.*, vol. **40**, p. 337, 1904.

[4] Carlson, E. T., *Bur. Standards J. Research*, vol. **9**, p. 825, 1932.

[5] The glass in this system richest in SiO_2 that has been described is that containing 89.2% (Greig, *op. cit.*, p. 139).

[6] Morey, G. W., and Merwin, H. E., unpublished results.

[7] Cousen, A., and Turner, W. E. S., *Jour. Soc. Glass Tech.*, vol. **12**, p. 169, 1926.

[8] The refractive index of SiO_2 glass is 1.458 (Sosman, *The Properties of Silica*). The index of B_2O_3 is dependent on heat treatment to an unusual degree, and it may range from 1.450 to above 1.460. Wulff P. and Majumdar S. K. (*Zeit. physik. Chem.*, **B31**, p. 319, 1936) consider that the best value of the refractive index of thoroughly dehydrated and annealed B_2O_3 glass is 1.4584; but the problem has not yet received definitive study.

The amount of CaO dissolved by the lighter layer in the ternary system is indicated by the following experiments. When 0.5% CaO was added to a homogeneous glass containing 60% B_2O_3, 40% SiO_2, the cooled glass appeared solidly white. With 0.25%, the glass appeared clear and homogeneous at 1400°, but became cloudy on cooling, at a temperature probably above 1000°. A mixture containing 0.1% CaO remained clear and transparent. It is concluded that the lighter liquid at 1000° contains less than 0.25% CaO, and as the temperature is raised the CaO-content is slightly increased.

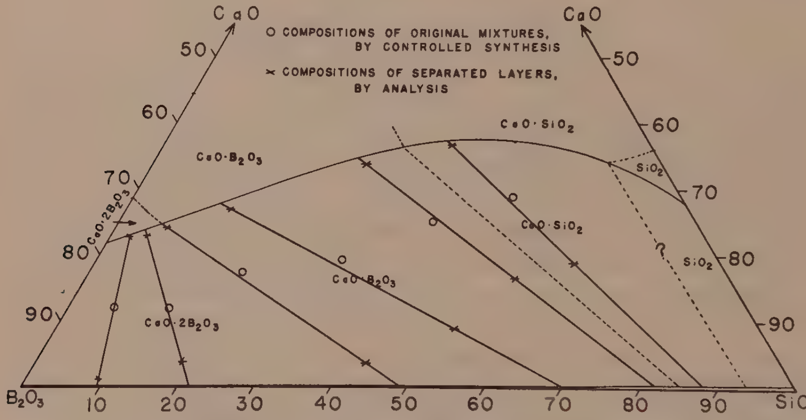

FIG. 1. The compositions of the mixtures used in determining the tie-lines, and of the two layers obtained for analysis. Each of the liquids contains some of the other phase, but the separation is much better in the CaO-rich layer.

The heavy liquid in the binary system, CaO–SiO_2, contains 27.5% CaO. As B_2O_3 is added this increases to a maximum of 38% CaO at a ratio of B_2O_3 to SiO_2 of 40% B_2O_3 to 60% SiO_2. The curve representing the composition of the heavier layer accordingly is concave toward the side B_2O_3–SiO_2, as shown in Fig. 1. For this reason it is possible to mix homogeneous glasses in the two limiting binary systems, CaO–SiO_2 and CaO–B_2O_3 containing less than 38% CaO and obtain two immiscible liquids.

On raising the temperature the CaO-content of the heavier liquid phase diminishes slightly, although the change is more evident than is the change in composition of the lighter layer. With increasing temperature the compositions of the two liquids tend to approach each other, and at a sufficiently high temperature it is possible that the two layers would disappear in the middle of the diagram, giving rise to two critical solutions and two separated regions of immiscibility.

The compositions which separate into two liquid layers are easy to determine by making up mixtures of varying composition and observing if they give clear glasses or contain globules of a second layer of differing refractive index. The determination of the coexisting liquids themselves, that is, of the direction of the tie-lines, is not so easy. It is necessary to prepare mixtures within the region of immiscibility, to make them as homogeneous as possible by repeated heating and grinding, and to allow the two layers to separate at a temperature a little above that of coexistence with a solid phase. The separation into two layers is not always satisfactory. Mixtures containing more B_2O_3 than SiO_2 are fluid enough to give a poor to fairly clean separation of the two layers, but mixtures rich in silica are so viscous that a clean separation is not possible. The difficulty is evident from the fact that the upper layer at the melting of danburite, 1000°, contains almost 85% silica. The several tie-lines determined are shown in Fig. 1 and the compositions in Table 1.

TABLE 1

THE COMPOSITIONS OF THE MIXTURES USED IN DETERMINING THE TIE-LINES, AND OF THE TWO LAYERS OBTAINED FOR ANALYSIS. EACH OF THE LIQUIDS CONTAINS SOME OF THE OTHER PHASE, BUT THE SEPARATION IS MUCH BETTER IN THE CaO-RICH LAYER

	SiO_2	CaO	B_2O_3
Original[1]	6.0	12.0	82.0
Upper	9.5	1.2	89.3[2]
Lower	2.4	23.0	74.6
Original	13.0	12.0	75.0
Upper	18.8	4.0	77.2
Lower	4.4	23.2	72.4
Original	19.7	17.7	62.6
Upper	42.5	3.9	53.6
Lower	6.1	24.2	69.7
Original	31.8	19.4	48.8
Upper	51.0	9.0	40.0
Lower	13.2	27.0	59.8
Original	40.7	25.3	34.0
Upper	55.5	16.8	27.8
Lower	27.7	34.1	38.2
Original	49.0	29.3	21.7
Upper	62.0	19.1	17.9
Lower	37.0	37.1	25.9

[1] All original compositions by controlled syntheses.

[2] B_2O_3 determined by difference in analyses of the upper and lower layers.

2. Coexistence with Crystalline Phases

When mixtures of the three components within the composition area of immiscibility are heated at sufficiently high temperatures, they separate into two liquid phases, and a vapor phase, consisting essentially of B_2O_3. This region is consequently divariant. When the temperature is lowered crystalline phases make their appearance; and the divariant region of immiscibility is bounded by several divariant regions representing equilibrium between solid, liquid and vapor. The line of contact between these regions represents equilibrium between four phases, and is consequently univariant. The compositions studied in outlining these fields, and the results of their study, are indicated in Fig. 2. The compositions of the mixtures and the details of their experimental study are given in Table 2.

Table 2

The Compositions of the Mixtures Used in Studying the Phase Equilibrium Relationships in and Adjacent to the Region of Immiscibility, and the Details of the Experimental Study

SiO_2	CaO	B_2O_3	Time	Temp.	Phases
2.0	23.7	74.3	30′	976.2	Glass
			45′	975.9	Glass
			30′	974.7	Glass+$CaO\cdot 2B_2O_3$
			45′	973.7	Glass+$CaO\cdot 2B_2O_3$
			45′	971.5	Glass+$CaO\cdot 2B_2O_3$
4.9	23.8	70.3	45′	972.3	Glass
			45′	971	Glass
			45′	969	Glass+$CaO\cdot 2B_2O_3$
			45′	968	Glass+$CaO\cdot 2B_2O_3$+$CaO\cdot B_2O_3$
6.9	24.8	68.3	30′	973	Glass
			1 hr.	972	Glass+$CaO\cdot B_2O_3$
			30′	968	Glass+$CaO\cdot B_2O_3$
10.2	30.6	59.4	10′	1029	Glass
			10′	1025	Glass
			10′	1023	Glass+$CaO\cdot B_2O_3$
			10′	1022	Glass+$CaO\cdot B_2O_3$
17.9	31.8	50.3	45′	1037	Glass
			45′	1034	Glass
			20′	1030	Glass+$CaO\cdot B_2O_3$

TABLE 2—(*Continued*)

THE COMPOSITIONS OF THE MIXTURES USED IN STUDYING THE PHASE EQUILIBRIUM RELATIONSHIPS IN AND ADJACENT TO THE REGION OF IMMISCIBILITY, AND THE DETAILS OF THE EXPERIMENTAL STUDY

SiO_2	CaO	B_2O_3	Time	Temp.	Phases
10.1	40.3	49.6	10′	1122	Glass
			10′	1101	Glass
			10′	1097	Glass+$CaO\cdot B_2O_3$
			10′	1095	Glass+$CaO\cdot B_2O_3$
			10′	1093	Glass+$CaO\cdot B_2O_3$
20.2	40.4	39.4	10′	1052	Glass
			15′	1051	Glass
			30′	1049	Glass+$CaO\cdot B_2O_3$
			30′	1047	Glass+$CaO\cdot B_2O_3$
			10′	1046	Glass+$CaO\cdot B_2O_3$
25	35	40	30′	1029	Glass
			1 hr.	1026	Glass
			1 hr.	1024	Glass+$CaO\cdot B_2O_3$
			30′	1022	Glass+$CaO\cdot B_2O_3$
24.9	39.8	35.3	45′	1034	Glass
			30′	1027	Glass
			30′	1020	Glass+$CaO\cdot B_2O_3$
			2 hr.	1019	Glass+$CaO\cdot B_2O_3$
			2 hr.	1017	Glass+$CaO\cdot B_2O_3$
29	36	35	30′	1017	Glass
			30′	1011	Glass
			30′	1009	Glass+$CaO\cdot B_2O_3$
			2 hr.	1007	Glass+$CaO\cdot B_2O_3$
30.3	40.4	29.3	10′	1007	Glass
			10′	994	Glass
			10′	992	Glass+$CaO\cdot SiO_2$
			10′	990	Glass+$CaO\cdot SiO_2$
			10′	985	Glass+$CaO\cdot SiO_2$
32.2	37.2	31.4	30′	982	2 glasses
			45′	980	2 glasses
			30′	979	2 glasses+$CaO\cdot SiO_2$+$CaO\cdot B_2O_3$
			30′	978.6	2 glasses+$CaO\cdot SiO_2$+$CaO\cdot B_2O_3$
			30′	978	2 glasses+$CaO\cdot SiO_2$+$CaO\cdot B_2O_3$

TABLE 2—(*Continued*)

THE COMPOSITIONS OF THE MIXTURES USED IN STUDYING THE PHASE EQUILIBRIUM RELATIONSHIPS IN AND ADJACENT TO THE REGION OF IMMISCIBILITY, AND THE DETAILS OF THE EXPERIMENTAL STUDY

SiO_2	CaO	B_2O_3	Time	Temp.	Phases
34.5	37.5	23.0	30′	1018	2 glasses
			1 hr.	1012	2 glasses
			30′	1011	2 glasses+$CaO\cdot SiO_2$
			30′	1007	2 glasses+$CaO\cdot SiO_2$
			20′	997	2 glasses+$CaO\cdot SiO_2$
40.2	37.1	22.7	14 hr.	1131	2 glasses
			1 hr.	1115	2 glasses
			1 hr.	1107	2 glasses+$CaO\cdot SiO_2$
			1 hr.	1097	2 glasses+$CaO\cdot SiO_2$
			1 hr.	1079	2 glasses+$CaO\cdot SiO_2$
39.0	38.6	23.4	25′	1104	Glass
			3 hr.	1088	Glass
			25′	1087	Glass+$CaO\cdot SiO_2$
			30′	1076	Glass+$CaO\cdot SiO_2$
			30′	1065	Glass+$CaO\cdot SiO_2$
39.2	39.2	21.6	30′	1156	Glass
			1 hr.	1147	Glass+$CaO\cdot SiO_2$
			1 hr.	1144	Glass+$CaO\cdot SiO_2$
			2 hr.	1133	Glass+$CaO\cdot SiO_2$
49.8	39.8	10.4	10′	1331	Glass
			30′	1312	Glass
			45′	1308	Glass+$CaO\cdot SiO_2$
			10′	1306	Glass+$CaO\cdot SiO_2$
			45′	1281	Glass+$CaO\cdot SiO_2$
49.5	36.2	14.3	1 hr.	1256	2 glasses+trace $CaO\cdot SiO_2$
			1 hr.	1248	2 glasses+$CaO\cdot SiO_2$
			1 hr.	1206	2 glasses+$CaO\cdot SiO_2$
55	35	10	1 hr.	1298	2 glasses
			30′	1294	2 glasses+$CaO\cdot SiO_2$
			2 hr.	1291	2 glasses+$CaO\cdot SiO_2$
			45′	1288	2 glasses+$CaO\cdot SiO_2$
			1 hr.	1283	2 glasses+$CaO\cdot SiO_2$
59.3	34.6	6.1	30′	1397	Glass
			30′	1377	Glass
			30′	1370	Glass
			30′	1367	Glass+$CaO\cdot SiO_2$
			1 hr.	1358	Glass+$CaO\cdot SiO_2$

TABLE 2—(*Continued*)

THE COMPOSITIONS OF THE MIXTURES USED IN STUDYING THE PHASE EQUILIBRIUM RELATIONSHIPS IN AND ADJACENT TO THE REGION OF IMMISCIBILITY, AND THE DETAILS OF THE EXPERIMENTAL STUDY

SiO_2	CaO	B_2O_3	Time	Temp.	Phases
61.3	33.8	4.9	1 hr.	1427	2 glasses
			40′	1409	2 glasses+SiO_2 (?)
			1 hr.	1387	2 glasses+SiO_2
			1 hr.	1368	2 glasses+SiO_2+$CaO \cdot SiO_2$

The compounds whose fields are adjacent to the region of immiscibility are: $CaO \cdot 2B_2O_3$, $CaO \cdot B_2O_3$, $CaO \cdot SiO_2$ and silica, in the forms of cristobalite and tridymite, respectively, above and below 1470°. The positions of the invariant points at which pairs of these compounds can coexist in equilibrium with two liquids are indicated in Fig. 2. These invariant points are quintuple points, and from each proceed five univariant equilibria. The sequence of *P-T* curves around the quintuple points may be deduced and correlated with the *T-X* diagram from general theory,[9] but in this case may be deduced from simpler considerations.

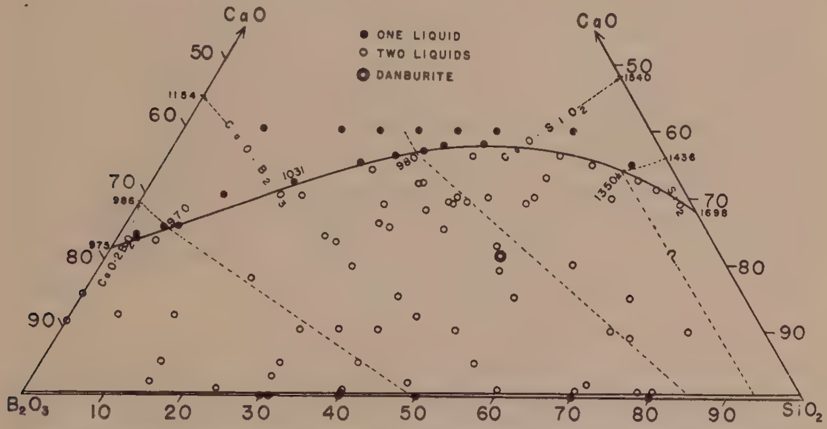

FIG. 2. The boundaries of the region of immiscibility and the adjacent fields, and the compositions of the mixtures used in their study.

From the quintuple point $V+L_1+L_2+CaO \cdot 2B_2O_3+CaO \cdot B_2O_3$, five univariant equilibria may be obtained by the disappearance of each one of the coexisting phases in turn. That obtained by the disappearance of the vapor phase, the curve showing the effect of pressure on the temperature and composition of the variable phases at the quintuple point, will not be considered. The equilibria obtained at this and the other quintuple points by the disappearance of the heavy liquid will be considered in detail later.

---

[9] Morey, G. W., and Williamson, E. D., *Jour. Am. Chem. Soc.*, vol. **40**, p. 59, 1918. Morey, G. W., *Jour. Franklin Inst.*, vol. **194**, p. 425, 1922.

The equilibrium obtained by the disappearance of the lighter liquid, $V+L_2+CaO\cdot 2B_2O_3+CaO\cdot B_2O_3$, terminates at the binary eutectic between these two solid phases, and the temperature must rise to the side of the diagram. Similarly, that obtained by the disappearance of $CaO\cdot B_2O_3$, the temperature of the equilibrium $V+L_1+L_2+CaO\cdot 2B_2O_3$, must rise from the quintuple point to the side of the diagram. Also, temperatures must rise along the curve $V+L_1+L_2+CaO\cdot B_2O_3$, because the maximum temperature along this curve will be at the point at which the three phases $CaO\cdot B_2O_3$, L_1 and L_2 lie on a straight line. This is at about 33% SiO_2. On further change in composition, temperature will fall, until the curve ends at the quintuple point $V+L_1+L_2+CaO\cdot B_2O_3+CaO\cdot SiO_2$. The other curves which proceed from this point are: $V+L_2+CaO\cdot B_2O_3+CaO\cdot SiO_2$, along which temperatures will rise toward the line joining the two compounds; and $V+L_1+L_2+CaO\cdot SiO_2$, along which the temperature will rise to its end at the quintuple point $V+L_1+L_2+CaO\cdot SiO_2+SiO_2$. Each of the curves representing equilibria in which a solid phase is present, the curves $V+L_2+CaO\cdot SiO_2+SiO_2$ and $V+L_1+L_2+SiO_2$, go to higher temperatures as they approach their ends on the side of the component triangle.

3. The Invariant Points of the Type $V+L_1+S_1+S_2+S_3$

In the preceding discussion of the invariant points of the type $V+L_1+L_2+S_1+S_2$, the univariant equilibria of the type $V+L_1+S_1+S_2$ have been omitted. These are obtained by the disappearance of the heavier liquid, and their prolongation must lie within the region between the side B_2O_3–SiO_2 and the curve giving the composition of the lighter liquid, as indicated diagrammatically in Fig. 3. It has been shown that this liquid contains only a small quantity of CaO, less than one-fourth of one per cent at about 50 per cent SiO_2, hence the field is exceedingly narrow. Nevertheless, within this narrow strip several important phase changes must take place.

Along each of the curves representing the univariant equilibria derived by the disappearance of the heavier liquid from the several invariant points, the temperature falls until the curve terminates at an invariant point of the type $V+L_1+S_1+S_2+S_3$. These curves bound fields within the area between the region of immiscibility and the side of the triangle, and there must be fields corresponding to each of the compounds adjacent to the curve giving the composition of the heavy liquid. These, in order of increasing SiO_2 content of the liquid, are: $CaO \cdot 2B_2O_3$, $CaO \cdot B_2O_3$, $CaO \cdot SiO_2$, and SiO_2.

The field of SiO_2 occupies a unique position. All the other crystalline phases in contact with the region of immiscibility are richer in CaO than the liquids in equilibrium with them. In the binary system, CaO–B_2O_3, the solid phase in equilibrium with the two liquids is $CaO \cdot 2B_2O_3$, the field of which must extend across the region of immiscibility, then fall to the (unknown) boundary of the field of crystalline B_2O_3, and the field of crystalline boric oxide cannot come into contact with the region of immiscibility. But in the binary system, CaO–SiO_2, the two liquid layers are in equilibrium with crystalline silica, cristobalite, the field of which extends on both sides of the area giving the composition of the two liquid phases. From the invariant point $V+L_1+L_2+CaO \cdot SiO_2+SiO_2$ the univariant equilibrium $V+L_1+CaO \cdot SiO_2+SiO_2$ will continue with falling temperature to its end-point at the invariant point $V+L_1+CaO \cdot B_2O_3+CaO \cdot SiO_2+SiO_2$. Below and to the right of the curve representing this equilibrium is the field of crystalline silica. Since silica must remain solid phase in the binary system, B_2O_3–SiO_2, until the binary eutectic is reached, the silica field extends from the SiO_2-apex until it meets the field of crystalline B_2O_3. At each of the invariant points of the type $V+L_1+S_1+S_2+S_3$ crystalline silica, in the form first of cristobalite, then of tridymite, then of quartz, is one of the coexisting solid phases.

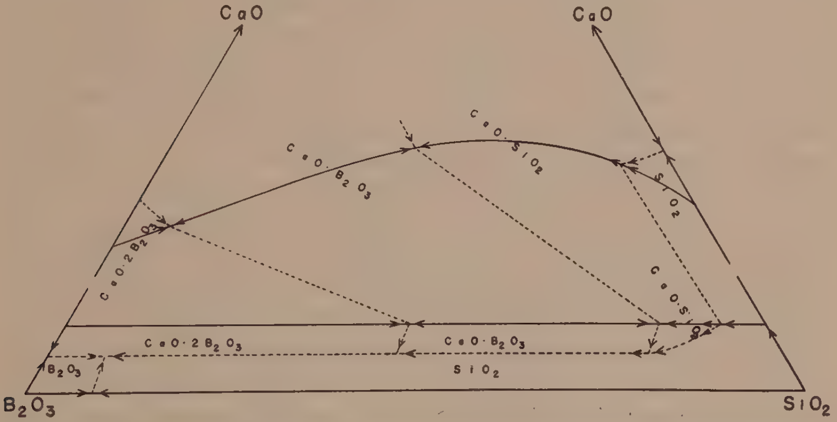

FIG. 3. Diagrammatic representation of the phase equilibrium relationships in the ternary system, CaO–B_2O_3–SiO_2, adjacent to the region of immiscibility.

In the narrow strip of compositions between the region of immiscibility and the side of the triangle there must, then, be a field of silica which continues to the field of B_2O_3, and between the silica field adjacent to the side and the curve giving the composition of the lighter liquid, fields of $CaO\ SiO_2$, $CaO \cdot B_2O_3$, and $CaO \cdot 2B_2O_3$.

We know nothing about the phase equilibrium relations in the binary system, B_2O_3–SiO_2, but from the isotherms and tie-lines in the ternary system we can make some inferences. In general the content of CaO along the boundary of the silica field cannot differ much from one-tenth of one per cent, and the CaO-content of the lighter immiscible liquid is not very different from one-fourth of one per cent. It is not probable that these "impurities" can greatly affect the freezing points, and hence that the liquidus temperatures in the binary system, B_2O_3–SiO_2, can differ much from those of the univariant equilibria $V+L_1+L_2+S_1$. From the direction of the tie-lines it is evident that the liquidus temperature must fall rapidly on addition of B_2O_3 to SiO_2, because the tie-lines terminating at about 10% B_2O_3 correspond to about 1000°. The lighter liquid at the invariant point $V+L_1+L_2+CaO \cdot 2B_2O_3+CaO \cdot B_2O_3$ contains about 55% B_2O_3, and the temperature is 900°. It is therefore to be expected that the tridymite liquidus in the binary system will be flat over the range from 10 to 55% B_2O_3, but from that point its further course is pure guesswork. The adjoining field is that of $CaO \cdot 2B_2O_3$, and the temperatures along the boundary of the two fields, the univariant equilibrium $V+L+CaO \cdot 2B_2O_3+SiO_2$, fall to the ternary eutectic at which crystalline B_2O_3 appears. This temperature is not known, but it must be low; and it may be that in the binary system, B_2O_3–SiO_2, the liquidus temperature will fall slowly until the SiO_2 content is low, then with increasing slope until it becomes almost vertical. It is a thermodynamic necessity that as the content of SiO_2 approaches zero the slope of the melting point curve shall approach infinity.

4. THE MELTING OF DANBURITE

The composition of danburite is in the region of immiscibility. The mineral remains unaffected by heating until 996°, when sintering begins. When left a long time—several days—at 1002°, the compound is entirely decomposed, with formation of two liquid layers. The crystalline compound is easily superheated, and is not entirely melted in an hour at 1000°.

The melting of danburite takes place at a temperature lower than corresponds to the univariant equilibrium $V+L_1+L_2+CaO \cdot B_2O_3$, and the heavy liquid should partially crystallize to calcium borate, with change in composition of both liquids. This series of reactions can be realized in part by long-continued heating, but complete attainment of equilibrium would require protracted heat treatment.

We have not been able to re-form danburite by heat treatment below the melting temperature, even though the materials were repeatedly finely ground and re-heated. Its synthesis is possible by hydrothermal means, and the effect of the addition of water and other components to this system is being studied.

A COMMON ORIENTATION AND A CLASSIFICATION FOR CRYSTALS BASED UPON A MARCASITE-LIKE PACKING

M. J. Buerger,
Massachusetts Institute of Technology, Cambridge, Mass.

Introduction

A marcasite-like arrangement of atoms is common to a rather large number of crystals. It is now desirable to organize the many data in this field for crystallographic purposes:

(a) by adopting a common orientation for these crystals based upon their structural *similarity*, and
(b) by providing a classification of these crystals based upon their structural *differences*.

These matters are treated in the present paper. It is also desirable to outline the fields within which the several structures may exist and the relations between these structures and the structures of neighboring fields. This crystallo-chemical discussion is reserved for a paper to appear shortly.

Orientation

It is now known that the arsenopyrite minerals definitely have marcasite-like crystal structures.[1] The ideal arsenopyrite structure is monoclinic, the false orthorhombic character of the group being caused by mimetic twinning on the pinacoids. The position of the 2-fold axis is parallel with the customary *c* axis. Since the 2-fold axis in monoclinic crystals is fixed by convention as the *b* axis, an axial interchange is required in the arsenopyrite group. A similar interchange is required in the axes of the truly orthorhombic marcasite and löllingite groups, in order to maintain the obvious relation between these groups and the arsenopyrite group. One of two alternative axial interchanges is necessary:

Old arsenopyrite orientation		New orientation required by the monoclinic character of ideal arsenopyrite	
		Alternative (1)	Alternative (2)
a	⟶	*a*	*c*
b	⟶	*c*	*a*
c	⟶	*b*	*b*

The marcasite-like packing is a generalization of the rutile packing.[2]

---

[1] Buerger, M. J., The symmetry and crystal structure of the minerals of the arsenopyrite group: *Zeit. Krist.*, (A) 95, pp. 83–113, **1936.**

[2] Buerger, M. J., The crystal structure of marcasite: *Am. Mineral.*, vol. **16,** pp. 392–393, **1931.**

It is therefore desirable, if possible, to make the new orientation of the marcasite-like minerals such that their structural orientations correspond with the rutile structural orientation. In the rutile structure, the metal coordination is octohedral. One of the important aspects of the packing is the linking of these octohedra into strings parallel with the 4-fold axis, by the sharing of edges. According to convention, the 4-fold axis is the *c* axis of tetragonal crystals, and this aspect of the structural orientation is therefore fixed. In the marcasite structure the direction of the strings of octohedra has been discovered to be parallel with the *a* axis of the arbitrarily chosen orthorhombic setting. To bring the marcasite-like minerals into conformity with the rutile setting, therefore, one of the following two alternative axial interchanges is necessary in the marcasite-like minerals:

Old marcasite orientation		New orientation required for correspondence with rutile structure	
		Alternative (I)	Alternative (II)
a	⟶	*c*	*c*
b	⟶	*b*	*a*
c	⟶	*a*	*b*

It will be observed that the old marcasite setting may be brought into harmony with both the symmetry requirement of arsenopyrite and the symmetry requirement of rutile because interchange alternatives (2) and (II) are identical. The axial interchanges for all crystals based upon a rutile-like or marcasite-like packing may now be summarized as follows:

		Old		New
for Rutile Group Hydrophylite Manganite	No interchange from customary orientation necessary.			
for Marcasite Löllingite Group Arsenopyrite Group		*a* *b* *c*	⟶ ⟶ ⟶	*c* *a* *b*

In the following discussion the *new* orientations are employed.

The Several Groups of Marcasite-Like Crystals

General.—All of the crystals discussed in this paper may be thought of as descending from the rutile structural type by either one, two, or three generalizations or specializations. These relations are summarized in Table 1. This table provides only some of the aspects which should be taken into consideration in the classification of these crystals; at least the AB_2 crystals are of several types.

Rutile group.—The rutile group requires little discussion in this place. The reader is referred, however, to the discussion bearing on the relation of this group to the marcasite group, which will appear in a subsequent contribution. The crystals belonging to the rutile group are listed in Strukturbericht.[3]

Marcasite group proper.—The marcasite group is usually made to cover not only marcasite but also the löllingite type and the arsenopyrite type crystals as well. Arsenopyrite is now known to have a different symmetry from marcasite as well as certain multiple axes. There is also a very real difference between marcasite and the löllingite crystals which should be recognized by placing them in different categories.

The difference between marcasite and the löllingite group is fundamentally due to the lack of chemical parallelism and consequent difference in bonding. This shows up in the shape of the octahedral coordination environment of the iron (or other corresponding metal atom), which, in turn, is reflected in the axial ratio, particularly the length of the *c* axis. In describing this difference, it is convenient to consider the octahedron as having an equator and poles, the shared edges of the octahedra consisting of one of the two opposite pairs of edges of the equator. In marcasite, contrary to a statement by Pauling and Huggins,[4] the shared edge is shortened, as indicated by the following figures[5] (and compared with $CaCl_2$, discussed beyond):

Edge	Edge length			
	marcasite, FeS_2		hydrophylite, $CaCl_2$	
equator edge, unshared	3.37Å		4.20Å	
		$\Delta = .24$		$\Delta = .31$
meridian edge, unshared (equator to pole)	av. 3.13		3.89	
		$\Delta = .17$		$\Delta = .34$
equator edge, shared	2.96		3.55	

The presence of a shortened shared edge is commonly regarded as a criterion for ionic crystals.[4] It is possible that marcasite is of partially ionic, and only partially of non-polar character, which would help to account for its abnormally large sulfur atoms, abnormally small iron atoms[6] and excessively great electrical resistance, all compared with pyrite. In part, the shortened shared edge may be due to the repulsion between the negatively charged surfaces of the unbonded atoms which approach one another across the shared edge.

---

[3] Ewald, P. P., and Hermann, C., *Strukturbericht* 1913–1928, pp. 155–158, **1931.**

[4] Pauling, Linus, and Huggins, M. L., Covalent radii of atoms and interatomic distances in crystals containing electron-pair bonds: *Zeit. Krist.*, (A) 87, p. 216, **1934.**

[5] Buerger, M. J., The crystal structure of marcasite: *Am. Mineral.*, vol. **16,** p. 391, **1931.**

[6] See, however, reference 1.

As a result of the lengthening of the unshared equatorial edge, the marcasite group proper is characterized by a c axis (new orientation) somewhat longer than the normal side of the coordination octahedron of the metal atom. The löllingite type is sharply distinguished from the marcasite type on this basis, as discussed in the next section. (See also Table 2.)

Hydrophylite has a marcasite-like packing although this is apparently unrecognized by van Bever and Nieuwenkamp,[7] who determined the structure. Originally described as $CaCl_2$, the mineral hydrophylite is now regarded as having the composition[8] $KCaCl_3$. Artificial material apparently of ideal composition, $CaCl_2$, may be prepared.[7] Nevertheless the formula may still be regarded as somewhat doubtful, and it is barely possible that this mineral may really have a manganite-like character.

The deviation of the hydrophylite structure from the rutile prototype is exceedingly slight and the crystals are therefore highly pseudo-tetragonal. The slight departure from the rutile structure is due to the slight deviation of the Cl atoms toward pairing. This appears to be due to the large Cl radius, i.e., the Ca:Cl radius ratio is small compared with the Fe:S radius ratio in marcasite. This is discussed further in a subsequent contribution.

The löllingite group.—The löllingite group is sharply distinguished from the marcasite group by being composed of coordination octahedra whose *unshared equatorial edges are greatly shortened.* The shared edge is correspondingly lengthened:[9]

Edge	Edge length		
	FeP_2	$FeAs_2$	$FeSb_2$
equator edge unshared	2.72Å	2.85Å	3.19Å
meridian edge unshared (equator to pole)	av. 3.20	av. 3.33	av. 3.67
equator edge shared	3.69	3.78	4.15

---

[7] van Bever, A. K., and Nieuwenkamp, W., Die Kristallstruktur von Calciumchlorid, $CaCl_2$: *Zeit. Krist.*, (A) 90, pp. 374–376, 1935.

[8] Dana-Ford, *A Textbook of Mineralogy*, 4th revised edition, p. 464, 1932.

[9] Buerger, M. J., The crystal structure of löllingite, $FeAs_2$: *Zeit. Krist.*, (A) 82, pp. 185, 1932.

The shortening of the unshared edge undoubtedly represents a bond between the B atoms across this edge (Fig. 1). It results in an excessively short c axis which distinguishes the morphology of the löllingite group from that of the marcasite group, a distinction which is clearly brought out by Table 2.

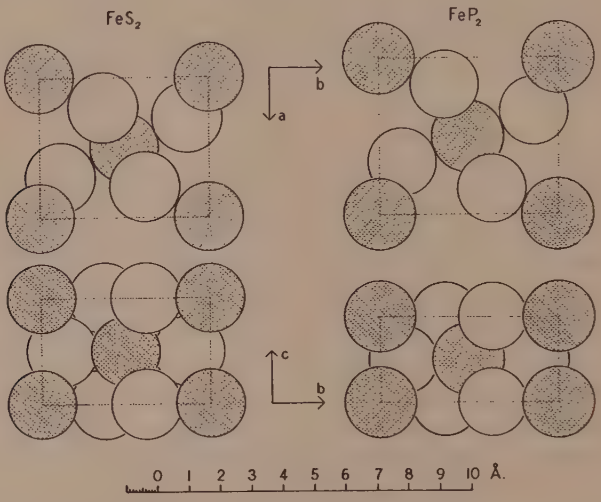

Fig. 1. The fundamental cause of the widely differing axial ratios of the marcasite group and the löllingite group. The illustration shows the plan and elevation of the unit cell of a representative of each group, the representatives being composed of isoperiodic atoms, i.e., the FeP_2 differs from the FeS_2 only by having its B atom one atomic number lower, and its valence therefore one greater. The additional valence causes the P atoms of the same iron coordination to bond themselves to one another in the c direction. This reduces the c dimension and increases a and b. The axial ratios of the two types of crystals are therefore distinct.

Key: shaded, iron atoms; unshaded, sulfur atoms (left diagram) or phosphorus atoms (right diagram). All atoms are drawn to scale from calculations from original crystal structure data.

Bäckströmite.—The existence of an hypothetical mineral, bäckströmite, $Mn(OH)_2$, has been deduced from orthorhombic pseudomorphs[10] now composed of pyrochroite. If bäckströmite truly represents a possible crystal, then the crystal structure is probably of the general marcasite type. The crystal structure is probably that of manganite with identity periods degenerate and symmetry raised due to the presence of identical B atoms. The hydrogen bonds probably exist along zigzag oxygen chains running in the direction of the *a* axis, connecting oxygens of different, as well as the same, cation coordinations.

---

[10] See discussion by Koechlin, R., in Doelter, C. and Leitmeier, H., *Handbuch der Mineralchemie*, III_2, pp. 845–846, **1926**.

The arsenopyrite group, gudmundite type.—Within the appropriate field, compounds corresponding with the ideal formula $AB'B''$ are monoclinic holohedral with doubled marcasite *a* and *c* axes.[11] This is here designated as the gudmundite type, for gudmundite displays the *x*-ray diffraction extinctions characteristic of this symmetry. Arsenopyrite itself is so prone to deviate from the ideal analysis that it usually falls into the next (triclinic) subdivision. Probably crystals of ideal monoclinic arsenopyrite exist, but investigation has not yet proceeded far enough to show this. The ideal monoclinic nature of gudmundite is apparently due to its relatively ideal composition, which, in turn, is probably due to the relatively great radius difference between $\mathrm{Sb}^{\mathrm{III}}$, on one hand, and $\mathrm{Fe}^{\mathrm{III}}$ and S on the other, which inhibits the proxying of one of these atoms by the other.

Manganite also probably belongs to the gudmundite type.[12] The $\mathrm{B}'-\mathrm{B}''$ pairing is caused in this crystal by an (OH)–O bond.

The arsenopyrite group, common arsenopyrite type.—The presence of ferric iron in arsenopyrite permits the arsenic and iron of the ideal formula to be replaced by one another freely.[13] Cobalt may also function as iron, and finally, arsenic may proxy for a certain amount of sulfur, which tends to make arsenopyrite approach the structure of löllingite. Apparently these replacements, especially the last, occur preferentially in alternate sheets, for the screw axes and glide planes which relate neighboring sheets to one another vanish, as shown by the substitutions of weak reflections for the extinct reflections required by the screw axes and glide planes. The common arsenopyrite is therefore triclinic. This is doubtless true also of the related species glaucodot, $\left|\begin{matrix}\mathrm{Co}\\\mathrm{Fe}\end{matrix}\right|\mathrm{AsS}$ and wolfachite, $\mathrm{Ni}\left|\begin{matrix}\mathrm{As}\\\mathrm{Sb}\end{matrix}\right|\mathrm{S}$. It is impossible to ascertain whether manganite rigorously belongs here or with the ideal gudmundite type, for its O and (OH) scatter *x*-rays identically, and a partial replacement of one by the other, which would render the structure triclinic, could not be detected.

---

[11] Buerger, M. J., The symmetry and crystal structure of the minerals of the arsenopyrite group: *Zeit. Krist.*, (A) 95, pp. 83–113, **1936.**

[12] Buerger, M. J., The symmetry and crystal structure of manganite, Mn(OH)O: *Zeit. Krist.*, (A), in press.

[13] Buerger, M. J., The symmetry and crystal structure of the minerals of the arsenopyrite group: *Zeit. Krist.*, (A) 95, pp. 110–111, **1936.**

Coordinated Crystallographic Data

In accordance with the discussion concerning common orientation and subdivision into groups, the crystallographic constants of the crystals based upon a marcasite-like packing are summarized in Table 2. Only constants based upon data obtained by x-ray methods have been used in this compilation. The accuracy of the values given is probably not very high, the limits of error lying between ±1% and ±.1%. Due to the common occurrence of solid solution, either of extraneous impurity atoms or of excess of one of the atoms already present in the ideal formula, it is not justifiable to quote values of greater apparent accuracy than those given in Table 2, unless the quotation applies to crystals of a definite locality or origin (i.e., composition).

Table 1

Derivation of Marcasite-like Crystals by Successive Specializations of Rutile Prototype

Formula type	Atomic specialization	Resulting crystallographic consequences	Crystal system	Crystals	
AB_2	(PROTOTYPE)		tetragonal	RUTILE GROUP	
AB_2	approach of B atoms in pairs	specialization of a_1 and a_2 axes to become a and b axes	orthorhombic	MARCASITE GROUP LÖLLINGITE GROUP BÄCKSTRÖMITE?	
$AB'B''$	specialization of 2 B atoms to become B' and B'' species	loss of symmetry and development of superstructure having a and c axes doubled	monoclinic	gudmundite type	ARSENOPYRITE GROUP
$\begin{array}{\|c\|c\|c\|}A & B' & B'' \\ X & Y & Z\end{array}$	preferential substitution of ideal formulary atoms by extra-formulary atoms in alternate (001) sheets	loss of screw axes and glide planes	triclinic	common arsenopyrite type	

The table brings out some interesting points: The distinction between the constants of the marcasite group and the löllingite group is striking, especially with regard to the ratio *c*:*b*, as illustrated in Fig. 1

TABLE 2

AXES AND AXIAL RATIOS (NEW ORIENTATION) OF CRYSTALS BASED UPON A MARCASITE-LIKE PACKING

Group		Member		Axes					
				absolute			ratio		
				a	*b*	*c*	*a*	*b*	*c*
RUTILE PROTOTYPE		rutile	TiO_2	4.58Å	4.58Å	2.95Å	1.000	1	.644
MARCASITE GROUP		hydrophylite	$CaCl_2$	6.24	6.43	4.20	.970	1	.653
		marcasite	FeS_2	4.44	5.39	3.37	.824	1	.625
LÖLLINGITE GROUP		iron diphosphide	FeP_2	4.97	5.67	2.72	.876	1	.480
		löllingite	$FeAs_2$	5.25	5.92	2.85	.887	1	$.481_5$
		iron diantimonide	$FeSb_2$	5.82	6.52	3.19	.893	1	.439
		safflorite	$CoAs_2$	—	—	—	—	—	—
		rammelsbergite	$NiAs_2$	—	—	—	—	—	—
ARSENOPYRITE GROUP	gudmundite type	gudmundite	$FeSbS$	10.04	5.93	6.68	1.694	1	1.126
		manganite	$Mn(OH)O$	8.86	5.24	5.70	1.690	1	1.088
	common arsenopyrite type	arsenopyrite	$FeAsS$	9.51	5.65	6.42	1.683	1	1.136
		glaucodot	$\left\|\begin{matrix}Co\\Fe\end{matrix}\right\|AsS$	9.62	5.73	6.67	1.678	1	1.164
		wolfachite	$Ni\left\|\begin{matrix}As\\Sb\end{matrix}\right\|S$	—	—	—	—	—	—

and for the reason discussed under *the löllingite group.* The löllingite group is an extraordinarily compact group showing slight and gradual variation of axial ratio with changing atomic radii. The marcasite group shows a much greater internal variation but it consists, as yet, of only two crystals composed of atoms of widely differing dimensions and bonding characteristics. When and if the group is expanded by the discovery of other members, it may be expected to show gradations.

The close agreement in axial ratio between manganite and the arsenopyrite minerals should also be observed. This, of course, is in good accord with the discovery that these have similar structures.

Finally, it should be pointed out again that the splitting of the arsenopyrite group into the gudmundite type and the common arsenopyrite type is a purely formal procedure based upon the fact that the chemically ideal type of this structure is monoclinic while the chemically impure type is triclinic. The relation is presumably a completely gradational one dependent upon impurity content. Alternatively, the relation between these two types may be looked upon as one in which the general case is triclinic, which degenerates to a special monoclinic case when the impurity content approaches zero.

CRYSTALLIZED POWELLITE FROM TONOPAH, NEVADA

FREDERICK H. POUGH, *American Museum of Natural History, New York City.*

Although powellite has been found at a number of localities, crystals have been reported only twice. It was originally identified and described as a new mineral by Melville,[1] who discovered it at the Seven Devils Mine in Idaho. He reported distinct crystals as much as 2.5 mm. across, although the average size was much smaller. After this determination, it was found at a number of localities, but always as a pulverulent coating, or in platy, pearly ocherous masses, pseudomorphous after molybdenite. The only other published descriptions of distinct crystals are those of the most notable occurrence to date; those of Houghton, Michigan. These were first noted by Koenig and Hubbard,[2] but more fully studied and figured by Palache,[3] who described two large and excellent crystals with several new forms.

With crystals of powellite as uncommon as this brief review shows, a suite collected at the Tonopah Divide Mine, near Tonopah, Nevada, is worthy of description. A considerable number of specimens was available for the study; in part borrowed from Harvard University through the kindness of Professor Charles Palache, and the remainder recently collected by Mr. C. D. Woodhouse, of Mocalno, California. The crystals occur in crusts, lining small vugs in an altered rhyolite and form a continuous layer of firmly intergrown individuals. The component crystals are small, averaging about 1.5 mm. in breadth, although some of the largest are as much as 5 mm. across. They differ greatly in habit and color. Some crusts show varying color tones, from a deep transparent brown, in the clearer portions of the crystals, to a milky brown on many of the surfaces where a thin skin composing the outer layer conceals the transparent interior. This skin appears to be very superficial and may be due to the presence of minute open spaces. Some crystals are half cloudy and half clear; the boundary line is abrupt and always runs vertically across the face, never parallel to the basal plane. The surfaces have an adamantine luster, but this, too, varies when the milky skin is present. The clearer crystals have brilliant faces marked by a series of striations running in the vertical plane across the face. The surfaces of the milky faces are much less brilliantly reflecting, show a somewhat rounded and irregular surface, and lack the distinct parallel striations.

---

[1] Melville, W. H., Powellite-calcium molybdate: A new mineral species. *Am. Jour. Sci.*, (3), vol. **41**, pp. 138–141, 1891.

[2] Koenig, G. A., and Hubbard, L. L., On powellite from a new locality: *Am. Jour. Sci.*, (3), vol. **46**, pp. 356–358, 1893.

[3] Palache, C., Powellite crystals from Michigan: *Am. Jour. Sci.*, (4) vol. **7**, pp. 367–369, 1899.

Other crusts, however, are very different in appearance, with pale yellow-brown and almost completely transparent crystals. In some the crystals are in parallel arrangement, either in a single group or in two or three units which compose the entire crust a centimeter or more across. Others show complete random orientation of the individuals. These paler crystals are more even and brilliant, are unstriated, and show very different forms and habits from those of the type first described. Some are pyramidal, while others are thinly tabular, resembling wulfenite crystals of this habit.

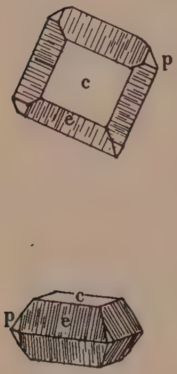

Fig. 1

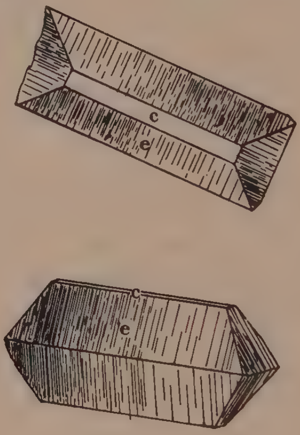

Fig. 2

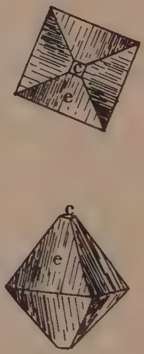

Fig. 3

The crystals forming the deep brown crusts show three variations of a pyramidal habit. The least common of these is that shown in Fig. 1, and is the usual habit of the smallest crystals, the ones about .3 mm. across. Such crystals were seen in smaller vugs or in fissures, but not on the larger and thicker crusts. The base is rather prominent, *e* is less striated than in the larger crystals and gives a good signal. The train-of-reflection is less continuous than in the other crystals and the form terminating the train, *p*, is better developed than is commonly the case. The base gives an excellent single reflection.

A more common habit is that shown in Fig. 2, which characterizes many of the larger brown crystals. The base is small and unimportant on these, which are dominated by *e*, and they are greatly distorted along an horizontal axis, so that two pairs of bipyramid faces are very much elongated in relation to the other pairs. The distribution of the striated planes makes the orientation of any of the distorted crystals very simple, however, and the forms are easily determined. As in the typical undistorted crystal shown in Fig. 3, the tetartohedry is pronounced. It reveals itself, even to casual inspection, through a rounding of the corners on the right or left sides of each *e* face, often grading into *p*. On the goniometer a continuous train-of-reflection is seen to extend from *e* through *h* and *r*, and on to *p*.

r (323) is a new form which was commonly observed on the pyramidal crystals of this group. It lies in the zone marked by the train-of-reflection and gives an intense and distinct signal in the train. *h* (313), first observed by Palache on a Michigan crystal, gives a similar signal in the train. No good forms were found between the base and the pyramids of the unit zone, although some apparent truncations were observed. They did not give good signals and cannot be considered acceptable forms.

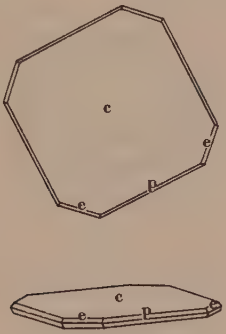

FIG. 4

Some new forms were found in this area, however, on some of the clearer pale-colored crystals. The crystals of this shade formed two widely divergent habit groups. One was tabular, some of the crystals paper-thin with the edges modified by *e* and *p*, the latter dominant; in marked contrast to the previously figured crystals on which *e* has been the broader form. No measurable forms lying between these and the base were observed. The faces of *e* and *p* are somewhat irregular, in the manner of wulfenite crystals of this habit, and do not give good signals. They are sufficiently good, however, for the determination of the forms. A typical crystal is shown in Fig. 4.

The most interesting of the crystals were the clear pyramidal ones, for they showed several new forms. The best developed and most perfect crystals consist of a simple combination of *c*, *e* and *p*, without other forms, but a few showed two additional very well-developed forms, *U* (137) and *u* (317);[4] as shown in Fig. 5. The faces of these complementary forms lie at the top of *e*, truncating that form at its intersection with the base. They form distinct pairs of faces, occurring thus four times on an end, no tetartohedry being apparent. The measured angles were:

$\phi=18^\circ 48'$ $\phi=71^\circ 12'$ $\rho=35^\circ 05'$

Calculated:

$\phi=18^\circ 26'$ $\phi=71^\circ 34''$ $\rho=34^\circ 57'$

Between these pairs, lying a little to the side of the [*cp*] zone, is another form which was observed four times on the crystal and which approaches very near to (4·3·14) in its symbol. Although it seems to be a new form on the crystal, it cannot be accepted without confirmation, because of the uneven measurements secured.

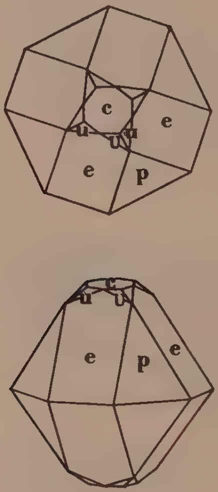

Fig. 5

Several other crystals of this type were measured and the *U-u* combination found on all of them. Most of these crystals were very irregularly developed, and did not form solid, regular bodies, but instead, showed uneven surfaces, on which, nevertheless, faces were regularly if unequally distributed. The crystals, and the new forms, are, for this reason, not figured, but excellent measurements were secured and four additional new forms made certain. These are: (123), (213), (319), and (113), lettered *F*, *f*, *x*, and *b*, respectively.

---

[4] (137) and a second new form (131), to be discussed later, were observed independently by Professor Palache in the course of some unpublished investigations.

	Measured:		*Calculated:*	
F	$\phi=26^\circ55'$	$\rho=49^\circ02'$	$\phi=26^\circ34'$	$\rho=49^\circ04'$
f	$\phi=63^\circ05'$	$\rho=49^\circ02'$	$\phi=63^\circ26'$	$\rho=49^\circ04'$
x	$\phi=71^\circ27'$	$\rho=27^\circ57'$	$\phi=71^\circ34'$	$\rho=28^\circ32'$
b	$\phi=45^\circ00'$	$\rho=35^\circ46'$	$\phi=45^\circ00'$	$\rho=36^\circ07'$

The last form, *b*, has already been noted upon artificial crystals, but this is the first natural occurrence of the form.

It is interesting to note that the pronounced tetartohedry of the mineral does not reveal itself in the distribution of forms lying within the unit distance, with the exception of *x* and one doubtful form. In the [$\bar{1}$01] zone, on the other hand, the tetartohedry is marked, and no complementary forms appear; a form is right or left, depending upon which end of the crystal is up. In order to avoid confusion it would be well to remember that this is the case; all of the forms in [$\bar{1}$01] lie in a single zone and if the zone is called [01$\bar{1}$] it makes no difference, as long as it is understood to contain all of the forms intersecting the *c*-axis at unity.

A careful measurement of the best crystals available showed that the ρ angle of the form *e* did not agree with that given for it in any of the published angle-tables. The results of thirty measurements on as many crystals were averaged to give a ρ angle for this form of 57°08′. Repeated attempts on two carefully selected very perfect crystals gave exactly the same value, so it was decided that a new axial ratio should be calculated, and new angles for the accepted forms. The following angle-table is calculated on the basis of a ratio of $a:c$ of 1:1.5477, or a p_0 of 1.5477, as are the calculated angles given in the above discussion. The angle-table is revised to include all of the accepted forms, including two, *S*(131), and *W*(153), which will be discussed later. All of the forms marked by an asterisk are new. All but *m*, *l*, *k* and *j* were observed during the course of this study.

The forms are listed according to usage and according to the increase in p, with a divergence from this practice in the case of complementary forms, in order to avoid a separation in the listing of forms which belong together. ϕ angles up to +90° suffice for all forms of this class; only in the case of the tetartohedral sphenoidal class will negative ϕ angles be necessary.

Note on Powellite from Houghton, Michigan

At the beginning of the preceding study, it was thought desirable for orientation purposes, to make a comparison of the appearance and reflections of the new crystals with one from the old Houghton locality. For this purpose, an excellent small crystal, attached to a quartz crystal, was removed from a specimen in the collection of the American Museum of Natural History. This crystal, a deep translucent blue one about 2 mm. across, showing touches of brown in transmitted light, gave excellent signals and a train extending from *e* to *p*, just as in the Nevada crystals described above. However, the crystal was found to be different

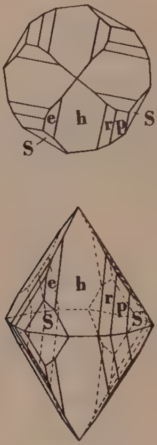

FIG. 6

from those described by Professor Palache, and to show a most unusual habit as well as two new forms. It is shown in Fig. 6. As may be seen, *e* is very narrow, but perfectly plane and brilliant, giving an excellent signal. The most prominent form, however, is *h*, which is dominant, making the crystal a little skewed from the axial directions. The signal from this form is blurred and covers several degrees in the train, the ρ angle naturally is much more exact than ϕ. A similar slightly attenuated signal next occurred in the train in the position of (323), already described on the Nevada crystals. The form is narrow, but well developed and but slightly rounded.

Measured:	*Calculated:*
$\phi = 56°25'$	$\phi = 56°19'$
$\rho = 60\ 50$	$\rho = 61\ 44$

The train ends with *p*, but further along in the same zone lies the comparatively large and very brilliant form *S* (131). This form was found six times on the crystal, three times on each end, and gave perfect signals.

Measured:	*Calculated:*
$\phi = 18°27'$	$\phi = 18°26'$
$\rho = 78\ 23$	$\rho = 78\ 27$

Because of these two new forms, as well as the unusual habit of the crystal, it was thought advisable to figure and describe this crystal as well.

POWELLITE
Angle-Table

$p_0 = 1.5477$ $a:c = 1:1.5477$

Form	Miller	φ	ρ
c	001	—°—′	00°00′
m	110	45 00	90 00
e	011	00 00	57 08
b*	113	45 00	36 07
p	111	45 00	65 27
U*	137	18 26	34 57
u*	317	71 34	34 57
x*	319	71 34	28 32
F*	123	26 34	49 04
f*	213	63 26	49 04
W*	153	11 19	69 11
l	11·1·11	84 48	57 14
k	515	78 41	57 38
j	11·3·11	74 45	58 04
h	313	71 34	58 30
r*	323	56 19	61 44
S*	131	18 26	78 27

NOTE ON POWELLITE FROM ISLE ROYALE MINE, HOUGHTON, MICHIGAN

C. PALACHE

A single crystal of powellite, found in a quartz vug from the Isle Royale Mine, was loaned to the writer for study by President McNair of the School of Mines at Houghton. This crystal was measured and the accompanying drawing made some thirty years since. The form and

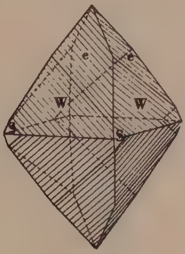

FIG. 7

peculiar striations of this crystal are so unusual that it seems well to take this occasion to put the observation on record. Unfortunately, the record of the angles obtained for the new form (153) can no longer be found. The crystal shows the forms *e* (101), *W* (153) and *S* (131). The form *S* is confirmed by Dr. Pough's work. The form *W* (153) was equally well founded and its good place in the projection, in spite of the loss of the record, makes the form seem worthy of recognition. The striation, in the direction of the edge $[2\bar{1}1]$, gives a highly skew appearance to the crystal.

SPECTROGRAPHIC EXAMINATION OF COLORLESS AND BLUE HALITE

T. G. Kennard,* David H. Howell and M. P. Yaeckel

The blue color sometimes observed in natural halite has been generally attributed to the effects of radiations,[1] although a number of investigators have advanced theories that pigments or impurities in the salt cause its color.[2] This spectrographic examination was made in order to ascertain whether or not any significant difference in chemical composition between the colorless and the blue varieties could be found. Since an examination of samples of smoky and colorless quartz obtained from the same specimen had shown that there was a difference in the lithium content,[3] it was expected that a difference in the composition of the blue and colorless portions of the halite might also be found.

The material examined was a specimen of colorless Stassfurt rock salt[4] containing a distinct zone of blue, which was irregular in outline. Samples of the colorless and of the blue halite were selected from adjacent regions of the interior portion of the specimen, and were found to be free from inclusions visible under a magnification of 35×. Minute, undetermined solid inclusions were found, however, under a magnification of 385×.

The method of preparing samples and determining color, and the spectrographic technique have been described.[5] However, Eastman

---

* Research Fellow in Chemistry, Claremont Colleges, Claremont, Calif.

[1] Among others: Przibram, *Sitzb. Akad. Wiss. Wien.*, Abt. IIA, vol. **138**, pp. 781–797; and pp. 483–495, 1929.

Przibram, *Kali*, vol. **17**, pp. 253–255, 1927.

Przibram, *Kali*, vol. **30**, pp. 61–63, 1936.

Przibram and Belar, *Sitzb. Akad. Wiss. Wien.*, Abt. IIA, vol. **132**, pp. 261–277, 1924.

Valentiner, S., *Kali*, vol. **6**, pp. 1–3; *N. Jahrb. Min. Geol.*, I, **1913**, Ref. 195.

Phipps, T. E., and Brode, W. R., *Jour. Phys. Chem.*, vol. **30**, pp. 507–520, 1926.

Lind and Bardwell, *Jour. Franklin Inst.*, vol. **196**, pp. 375–390, 1923.

[2] Among others: Doelter, C., *Sitzb. Akad. Wiss. Wien.*, Abt. I, vol. **138**, pp. 113–124, 1929.

Doelter, C., *Min. Petr. Mitt.*, vol. **38**, pp. 456–463, 1925.

Doelter, C., *Monatsch.*, vol. **52**, pp. 241–252, 1929.

Kreutz, F., *Zeit. Krist.*, vol. **24**, p. 626, 1895.

Focke, F., *Tsch. Min. Mitt.*, vol. **25**, p. 50, 1906.

Prinz, W., *Bull. Soc. Belg. Geol.*, vol. **22**, pp. 63–82, 1908; *N. Jahrb. Min. Geol.*, **1909**, II, Ref. 187–188.

[3] Kennard, T. G., *Am. Mineral.*, vol. **20**, pp. 392–399, 1935.

[4] The halite was obtained from R. M. Wilke, Palo Alto, Calif.

[5] Kennard, T. G., and Howell, David H., *Am. Mineral.*, vol. **21**, pp. 721–726, 1936.

spectroscopic plates, type I–F, were employed for photographing the visible spectrum. Specimens 1 cm. thick were used in determining the color.

TABLE OF RESULTS

Sample Number	Color	Ridgway's Standard[6]	Large	Very Small	Trace	Minute Trace
1.	Colorless	—	Na	Ca	Al Li K Si Ti	Mg Sr Ba
2.	Blue	48 e	Na	Ca	Al Li K Si Ti	Mg Sr Ba

Comparison of the spectra of the colorless and the blue halite shows that no difference in composition, as regards chemical elements, was detected spectrographically. The method used would not, of course, enable one to distinguish between sodium present as the chloride and sodium present as colloidal metallic sodium. No evidence was found to support the theory that the color of blue halite is due to a pigmental impurity.

With the exception of strontium, titanium and barium, the elements found are those which are generally present and have been reported in halite.[7]

The indices of refraction of the blue and colorless portions were identical within the limit of error of measurement, which was ± 0.002. This agrees with the results given by Doelter.[8]

SUMMARY

1. Colorless and blue halite have been examined spectrographically.
2. No difference in chemical composition was observed between the colorless and the blue varieties which had been obtained from the same specimen.
3. The blue color is structural rather than pigmental.

---

[6] Ridgway, *Color Standards and Color Nomenclature*, Washington, 1912.

[7] Doelter, C., *Hand. d. Mineralchemie*, vol. IV, Pt. 2, pp. 1028–1032, 1929.

[8] Doelter, C., *ibid.*, p. 1090.

4. The presence of strontium, titanium and barium in halite is reported.

There has been issued recently by the New Mexico School of Mines, Bulletin No. 11, The Geology of the Organ Mountains with an account of the geology and mineral resources of Dona Ana County, New Mexico. The author is Kingsley Charles Dunham, Commonwealth Fund Fellow, Harvard University. The price of this publication is $1.00. Orders should be sent to Dr. E. H. Wells, Director of the State Bureau of Mines and Mineral Resources, Socorro, New Mexico.

BOOK REVIEWS

RUTLEY'S ELEMENTS OF MINERALOGY by H. H. READ. 23rd edition. VIII+490 pages, 128 figures. Thomas Murby & Co., London. 1936. Price 8/– net.

A comparison of the twenty-third edition of this well-known Mineralogy with the preceding edition will reveal numerous marked changes. The size of the book has been increased by approximately 100 pages and 48 new illustrations have been added. The entire book has been reset which has made it possible to incorporate new material throughout the whole text, but the expansion is particularly note-worthy in Chapters III and IV, devoted to "Elements of Crystallography" and "The Optical Properties of Minerals." A new chapter has also been added on "The Occurrence of Minerals," which includes a classification and brief discussion of the main rock-types.

As in the previous edition the book is divided into two main divisions. Part I, "Properties of Minerals," and Part II, "Description of Minerals." In Part II the former classification has been changed and the one now followed stresses the economic phase by making use of groupings in which some important element is common to the entire group.

No attempt has been made to discuss crystal structure as revealed by x-ray analysis, but in other respects the book has been greatly improved and rendered more serviceable.

W. F. H.

PROSPECTING AND OPERATING SMALL GOLD PLACERS, Second edition, by WILLIAM F. BOERICKE. John Wiley & Sons, Inc., New York. 1936. Price $1.50.

This handbook in its first edition was written to assist the man, without technical education, in prospecting small placer deposits intelligently and to suggest means for equipping and operating placers at minimum cost, chiefly by home-made methods. The same objective is retained and is undoubtedly achieved in the new edition. The book is not only very readable for the uninitiated but contains much of value to the more experienced. The change in the price of gold from the old statutory figure of $20.67 per ounce to $35 makes necessary the revision of many statements in the first edition. The chapter on placer mining machines has been entirely rewritten and brought up to date with descriptions of a few new machines that have demonstrated their merit through hard use in the field.

A. J. EARDLEY

PROCEEDINGS OF SOCIETIES

MINERALOGICAL SOCIETY OF GREAT BRITAIN AND IRELAND

Anniversary Meeting, November 5th, 1936

The following were elected officers and members of Council: *President*, DR. L. J. SPENCER C.B.E., F.R.S.; *Vice-Presidents*, PROF. P. G. H. BOSWELL, AND MR. T. CROOK; *Treasurer*, MR. F. N. ASHCROFT; *General Secretary*, MR. W. CAMPBELL SMITH; *Foreign Secretary*, PROF. A. HUTCHINSON; *Editor of the Journal*, DR. L. J. SPENCER; *Ordinary members of Council:* PROF. A. BRAMMALL, MR. C. W. MATHEWS, DR. T. C. PHEMISTER, MR. A. BROUGHTON EDGE, PROF. H. H. READ, MR. ARTHUR RUSSELL, MR. R. C. SPILLER, DR. GILBERT WILSON, DR. A. F. HALLIMOND, PROF. C. E. TILLEY, MR. B. W. ANDERSON, MR. M. H. HEY.

DR. L. J. SPENCER, PRESIDENT, IN THE CHAIR

Prof. C. E. Tilley exhibited pyroxmangite- and rhodenite-bearing schists from the Lewisian of Glenelg; and Dr. A. T. Dollar an integrating stage for micrometric analysis.

(*1*) *Demonstrations in petrogenesis from Kiloran Bay, Colonsay. 1. The transfusion of quartzite.* By Miss D. L. REYNOLDS. (With analyses by Lady Agnes Gibbs and others.)

The hornblendite of three small composite intrusions is thickly sprinkled with blocks of white quartzite, most of which exhibit various stages of replacement by micropegmatite, syenite, and appinite. The syntectic rock types, which present an igneous appearance, occur in individual xenoliths either separately or in concentric zones. In the latter case micropegmatite or syenite adjoins the centrally placed residual core of quartzite. The boundaries between the residual quartzite and its replaced portion and between successive replacement zones are always sharp. Completely replaced xenoliths are represented by felspathic patches and schlieren. By study of successive replacement zones and chemical analysis, it is found that the process of replacement involved the differential diffusion of various magmatic constituents (possibly ionic) into the quartzite, some constituents having actually become concentrated in the metasomatic rocks.

Finally, the process of transfusion gave rise to syntectic magma of syenitic and appinitic composition, now represented by veins which emerge from metasomatized quartzite.

(*2*) *Transfusion of quartz xenoliths in alkali basic and ultrabasic lavas, south-west Uganda.* By Professor ARTHUR HOLMES. (With microchemical analyses by Dr. Hecht.)

Many of the lavas of south-west Uganda contain augite-rimmed xenoliths of transfused quartz. Transfusion begins with the development of intergranular channels of glass and continues until only isolated relics of quartz remain. Refractive indices: glass from various xenoliths, 1.472 to 1.497: pure silica-glass, 1.458. In order to ascertain what constituents migrated from magma to quartz, Dr. F. Hecht has made microchemical analyses of three samples of glass from pure quartzite or vein-quartz occurring in two murambites and a katungite from the Bufumbira district.

Analyses of these new rock-types are presented. Murambite is melanocratic leucite-absarokite. Katungite is potash-rich pyroxene-free olivine-melilitite. The results show that in all three rocks the glass has the composition of silica-rich potassic obsidian. The constituents introduced were mainly Al_2O_3, K_2O, and H_2O, accompanied by smaller amounts of Na_2O, TiO_2, P_2O_5, MnO, and the cafemic oxides. SO_3 was a notable contribution from murambite and CO_2 from katungite.

(3) *An occurrence of greenalite-chert in the Ordovician rocks of the southern uplands of Scotland.* By Mr. W. Q. Kennedy.

A dark-green to black cherty rock from the Arenig outcrop near Glenluce, Wigtownshire, is found to consist of rounded or irregular granules of a greenish, isotropic, amorphous mineral embedded in a fine-grained base of cherty silica. The optical properties, nature of the alteration, and composition of the rock indicate that the mineral is a pure hydrated ferrous silicate identical with the greenalite occurring in the Biwabik iron formation of Minnesota.

(4) *The composition and paragenesis of the biotites of the Carsphairn igneous complex.* By Mr. W. A. Deer (communicated by Prof. C. E. Tilley).

Three biotites have been analysed from the granites, tonalite, and hornblende hybrid of the Carsphairn intrusion. Their compositions are closely related to the enclosing rock when the mineral has crystallized under normal magmatic conditions. During the hybridization process this relationship is less strong due to changing equilibrium conditions. Their structural formulae, derived from partial x-ray analysis, have been calculated, and the formula suggested by Pauling is accepted in preference to Mauguin's. The $\mathrm{X}n$ group (co-ordination number 6) varies from $n=2.5$ to 3. In biotites from the intermediate rocks n approaches 3, and the mica becomes richer in the phlogopitic molecule. The biotites are related as members within a single intrusion and show characteristic features distinguishing them from biotites of other complexes.

NEW YORK MINERALOGICAL CLUB

50th Anniversary Celebration Banquet, November 18, 1936

The Club celebrated the 50th Anniversary of its existence with a large dinner, held in the "Birds of the World Hall," in the American Museum of Natural History on Nov. 18, 1936. Over 125 members and guests were present.

After the dinner and the President's address of welcome, Professor A. H. Phillips presided as toastmaster and introduced the speakers. Prof. B. T. Butler first spoke of the present club membership and their contributions in the field of mineralogy, despite their primary interests in other fields. The names of many distinguished men may be found upon the club's roster.

Mr. Gilman S. Stanton then continued speaking in the same vein, telling of some of the founders of the club and their places in the history of mineralogy in this country. The names of many of the members and all but one of the honorary members are perpetuated in mineral names.

Mr. H. P. Whitlock then spoke of some of the minerals which have been named for members of the club, notably bementite, canfieldite, roeblingite, kempite, hiddenite and kunzite. The most famous of our American mineralogists and one who assuredly deserves to have a mineral named for him, Edward Salisbury Dana, long an honorary member, has never been so memorialized, and Mr. Whitlock proposed that his middle name be used in this way.

Mr. E. N. Cameron, speaking for Prof. Paul F. Kerr, then demonstrated by projection, some very fine interference phenomena produced by orientated sections cut through different minerals. The unusual appearance of the brookite figure was shown. A final demonstration was made with a gypsum plate which was heated until it became uniaxial, reverting to its original large 2V on cooling.

The final speaker of the evening was Mr. O. Ivan Lee who demonstrated his discovery of the reversible photosensitivity of hackmanite, making the first public announcement of this discovery. The demonstration was very startling and impressive, and Mr. Lee's explanation of the cause was received with interest.

F. H. Pouch, *Secretary*

PHILADELPHIA MINERALOGICAL SOCIETY

Academy of Natural Sciences of Philadelphia, October 1, 1936

Mr. Harold W. Arndt presided at a stated meeting, 48 members and 30 visitors being present. The following officers were elected: *President:* Harold W. Arndt; *Vice-President:* Dr. Joseph L. Gillson; *Secretary:* Wylie H. Flack; *Treasurer:* Morrell G. Baldwin; and *Councillor:* Charles R. Toothaker.

Mr. A. Wm. Postel of the Department of Geology of the University of Pennsylvania gave an illustrated talk on "The Geology of Southern California."

Trips were reported by: Samuel G. Gordon (Perkiomenville) exhibiting stilbite; Harry W. Trudell (Bernardville, N. J., Tilly Foster, N.Y., Westfield, Mass., and Portland, Conn.) collecting beryl, tourmaline, albite, apatite, and fluorite; Lawrence Weagle (Nova Scotia); Arnold Morris (Beatty Road) beryl and ilmenite; Adolph E. Meier (quarry below Crum Creek Falls) molybdenite and beryl; Louis Moyd (Easton and Boyertown) molybdenite, hematite; G. Earle Thompson (Bridgeport, Penn.) malachite, calcite, quartz; Leonard Morgan (Prospect Park, Paterson, N.J.), agate, quartz, and datolite; Edwin Roedder (Hillburn, N.Y.) pyrite; Charles R. Toothaker (Judds Bridge, Conn.) cyanite; Constantine Challis (Phoenixville, Penn.) pyromorphite and wulfenite, (Leiperville) beryl and garnet.

W. H. Flack, *Secretary*

NEW MINERAL NAMES

Parawollastonite

M. A. Peacock: On wollastonite and parawollastonite. *Am. Jour. Sci.*, [5] vol. **30**, pp. 495–529, 1935. Peacock distinguishes two forms of wollastonite with the following properties:

	Wollastonite	Parawollastonite
	Triclinic	Monoclinic
$a:b:c$	1.0816:1:0.9649	1.0524:1:0.9649
	$\alpha=90°$	$\beta=95°24\frac{1}{2}'$
	$\beta=95°16'$	
	$\gamma=103°22'$	
p_0	0.9169	0.9169
q_0	0.9874	0.9606
	$\mu=84°35\frac{1}{2}'$	$\lambda=88°45'$
		$\mu=84°35\frac{1}{2}'$
	$\nu=76°34\frac{1}{2}'$	
X	1.620	1.620
Y	1.632	1.631
Z	1.634	1.633
$X \wedge c$	$31\frac{1}{2}° \pm 3°$	$34° \pm 3°$
$Y \wedge b$	$4° \pm 1°$	0
$2V$	$39° \pm 3°$	$44° \pm 3°$
Occurrence	Contact metamorphic	In ejected blocks.

W. F. Foshag

Earlandite

F. A. Bannister: Report on some crystalline components of the Weddell Sea Deposits. *Discovery Reports*, vol. **13**, pp. 67–69, 1936, with plate.

Name: In honor of Mr. Arthur Earland, in recognition of his contributions to the study of ocean deposits.

Chemical Properties: Hydrated calcium citrate; $Ca_3(C_6H_5O_7)_2 \cdot 4H_2O$. Analyses: (by E. Hope, on 3.6 mgs.) C 24.01, H 3.48, CaO 28.63, (by M. H. Hey on 1.8 and 4 mgs.) CaO 31.6 and 29.01. Soluble in dilute acid and decolorizes permanganate solution.

Physical and Optical Properties: Color pale yellow to white. $n=1.56$. $G=1.80$–1.95.

Occurrence: As very fine grained nodules, $\frac{1}{2}$–$1\frac{1}{2}$ mm. in diameter, also larger fragments, in the sediments of Weddell Sea from a depth of 2580 meters, associated with quartz grains, foraminifera, etc.

W. F. F.

Unnamed

F. A. Bannister: Report on some crystalline components of the Weddell Sea deposits. *Discovery Reports*, vol. **13**, pp. 60–66, 1936.

Chemical Properties: Probably calcium oxalate trihydrate, $CaC_2O_4 \cdot 3H_2O$. (From comparisons with the artificial salt and the presence of lime.)

Crystallographical Properties: Tetragonal, bipyramids $c{:}r=30\ \ 35'$. $a=12.40$, $c=7.37\pm0.02$ Å. $c=0.594$. Space group $C^5_{4h}=I\,4/m$.

Physical and Optical Properties: Transparent, colorless. $\omega=1.523$; birefringence 0.02.

Occurrence: Found sparsely distributed in the sediments of Weddell Sea at depths from 4434–5008 meters, as minute "envelope" crystals.

W. F. F.

Brickerite

F. Ahlfeld and R. Mosebach: Brickerite, ein neues Mineral. (Beiträge zur Geologie und Mineralogie Boliveins, Nr. 8.) *Centr. Mineral.*, Abt. A, No. **8**, pp. 226–231. 1936.

Name: From the owner of the Lilli Mine, David G. Bricker.

Chemical Properties: An arsenate of zinc and calcium: $Zn_4Ca_3As_4O_{17}$. Analysis: (by Dr. J. Barrande-Hesse). CaO 14.84, ZnO 29.07, Fe_2O_3 0.66, SiO_2 1.65, As_2O_5 40.84, $CaCO_3$ 10.46. Total 97.52.

Physical and Optical Properties: Color white. Luster silky. Cleavage parallel to the needles, with a transverse parting. Hd. 4. G. 4.13.

Biaxial, positive. $\alpha=1.752$, $\beta=1.7555$, $\gamma=1.779$. $2V=41°$.

Occurrence: Found in veinlets and nodules in tuff, with quartz, chalcedony and calcite as a hydrothermal spring deposit.

W. F. F.

F. Ahlfeld and R. Mosebach: *Ibid*, No. **9**, p. 287.

Comparison of optical and physical properties suggests the identity of brickerite and austinite. (Cf. *Am. Mineral.*, vol. **20**, p. 112, 1935.) A new analysis is promised.

W. F. F.

Metakernite

Heinrich Menzel, H. Schulz, H. Deckert: Bildungs- und Existenzbedingungen des Kernit, $Na_2B_4O_7 \cdot 4H_2O$. *Naturwiss.*, vol. **23**, pp. 832–833, 1935.

The sodium tetraborate dihydrate, $Na_2B_4O_7 \cdot 2H_2O$ formed from kernite by treatment with dehydrating agents or thermal treatment (100–120°) and which will regenerate to kernite with water vapor is called metakernite.

W. F. F.

DISCREDITED SPECIES

Gosseletite

F. Corin: Identité probable de la gosseletite et de la viridine (manganandalusite) occurrence de la viridine á Salm-Chateau. *Ann. Soc. Geol. Belg.*, vol. **57,** Nos. 8 and 9, pp. 152–157, 1934. (Cf. *Am. Mineral.*, vol. **13,** p. 593, 1928.)

A comparison of the properties of gosseletite with those of the viridine of Darmstadt suggests the probable identity of these two minerals. New data are given on the absorption spectra, as follows:

γ = two bands in the green at 550$\mu\mu$, and at 555$\mu\mu$ and 560$\mu\mu$.

β = near the limit of the blue extending from 496 to 505$\mu\mu$, and another at 550$\mu\mu$.

α = same as for γ but more indistinct.

W. F. F.

Matildite

P. Ramdohr: Bleiglanz, Schapbachite, Matildite. *Fortsch. Mineral.*, vol. **20,** pp. 56–57, 1936.

Mineralographic studies of matildite and schapbachite show them to be regular intergrowths of a predominately rhombic, weakly birefracting mineral, with a well defined pseudo-cubic lamellar structure, and galena. The compound $AgBiS_2$ is considered dimorphous: α $AgBiS_2$, a cubic high temperature form, and β $AgBiS_2$, an orthorhombic low temperature form. The name matildite should be dropped in favor of schapbachite.

W. F. F.